

Relativistic mean motion resonanceHuan Yang^{1,2}, Béatrice Bonga,² Zhipeng Peng,^{3,2} and Gongjie Li⁴¹*University of Guelph, Guelph, Ontario N2L3G1, Canada*²*Perimeter Institute for Theoretical Physics, Waterloo, Ontario N2L 2Y5, Canada*³*Gravitational Wave and Cosmological Laboratory, Department of Astronomy, Beijing Normal University, Beijing 100875, China*⁴*Center for Relativistic Astrophysics, School of Physics, Georgia Institute of Technology, Atlanta, Georgia 30332, USA*

(Received 21 October 2019; published 26 December 2019)

Mean motion resonances are commonly seen in planetary systems, e.g., in the formation of orbital structure of Jupiter's moons and the gaps in the rings of Saturn. In this work we study their effects in fully relativistic systems. We consider a model problem with two stellar mass black holes orbiting around a supermassive black hole. By adopting a two timescale expansion technique and averaging over the fast varying orbital variables, we derive the effective Hamiltonian for the slowly varying dynamical variables. The formalism is illustrated with a $n_\phi:n_r:n_\psi = 2:1:-2$ resonance in Schwarzschild spacetime, which naturally becomes the 3:2 resonance widely studied in the Newtonian limit. We also derive the multibody Hamiltonian in the post-Newtonian regime, where the radial and azimuthal frequencies are different because of the post-Newtonian precession. The capture and breaking conditions for these relativistic mean motion resonances are also discussed. In particular, it is possible that pairs of stellar mass black holes surrounding the supermassive black hole are locked into resonances as they migrate toward the supermassive black hole. As the inner object enter the LISA band, the outer object could reside at a close distance that significantly affects the inner object's gravitational waveform.

DOI: [10.1103/PhysRevD.100.124056](https://doi.org/10.1103/PhysRevD.100.124056)**I. INTRODUCTION**

Mean motion resonance is a type of orbital resonance that occurs when the orbital frequencies of two gravitationally interacting bodies, both moving in the gravitational potential well of a massive object, become commensurate with each other [1]. During these resonances, the mutual gravitational influence of the bodies is enhanced. As a result, mean motion resonances can significantly alter the orbit of one or both of the bodies. Depending on the eccentricity and/or the relative inclination of the two bodies, they can be captured into various resonance configurations. Some of these configurations are stable, such as the orbits of Pluto and the plutinos [2,3]; and some are unstable, such as the Kirkwood gaps in the asteroid belt at ~ 3 AU from our Sun [4,5]. Stabilization may occur when the two bodies are synchronized such that they never closely approach each other, in which case the resonance is locked. Once a pair or even a chain of objects [6] are locked into mean motion resonance, they can migrate together toward the central massive object while keeping the ratio of orbital frequencies fixed. The resonant locking breaks down if the adiabatic evolution of the trajectory in the phase space exits the resonance zone, or if the external dissipative force becomes stronger than the resonant interaction between the objects so that adiabatic approximation is no longer valid.

As all previous studies of mean motion resonances are performed within the Newtonian regime, it is interesting to extend the analysis of these resonances to the relativistic setting. A possible scenario in which relativistic effects may become important is when two stellar-mass black holes are orbiting a massive black hole. This would be a multiple EMRI (extreme mass-ratio inspiral). While EMRIs have not been observed yet, they are possible sources for the space-born gravitational wave detector, LISA (Laser Interferometric Space Antenna), which is scheduled to launch in 2034. As EMRI systems generally orbit 10^4 – 10^5 cycles in the LISA band before their final plunge, any additional force or small deviation from theoretical predictions may accumulate over many cycles resulting in an amplification of the deviation. Therefore EMRIs are ideal for testing the spacetime of rotating black holes in general relativity [7],¹ searching for the possible existence

¹However, many modified theories of gravity naturally contain coupling coefficients with negative mass dimensions due to the inclusion of higher derivative terms in the action, e.g., dynamical Chern-Simons theory [8] and Gauss-Bonnet theory [9]. Therefore for these theories the deviation from GR is amplified with lower-mass compact objects, and it would be preferable to use high-frequency gravitational-wave detectors [10,11] instead of LISA to obtain better constraints.

of an ultralight axion field [12–15] or other exotic matter/horizon structure [16–18], studying the physics of black hole accretion disks [19,20] and the astrophysical environment of supermassive black holes in galactic centers [21,22].

An important difference between geodesic orbits in general relativity (GR) and Newtonian orbits is the number of independent orbital frequencies. Geodesics around rotating black holes naturally contain three orbital frequencies, as compared to one orbital frequency for Newtonian Keplerian orbits. Therefore, the Newtonian condition for resonance to occur, i.e.,

$$j\omega + \underline{j}\underline{\omega} \approx 0 \quad (1.1)$$

with j, \underline{j} both integer and $\omega, \underline{\omega}$ describing the orbital frequency of the two bodies revolving around the massive object, is a subspace of the resonance condition in the relativistic scenario, which is a constraint on six orbital frequencies. In other words, the mutual gravitational interaction between different degrees of freedom (d.o.f.) allows a larger set of commensurate frequencies in GR. As a result, we expect a richer resonant structure than in Newtonian gravity. This is indeed the case, as we will see in Sec. II.

Resonant pairs are most likely to form in the Newtonian regime when both objects are far away from the massive black hole. This can happen, for instance, when both objects move within an accretion disk around the massive black hole. Such capture is similar to the standard planetary resonance capture mechanism. After capture into resonance, these pairs will jointly migrate toward the massive black hole by gravitational wave radiation and disk dissipation. As the resonant pair enters the strong-gravity regime, relativistic corrections start to play a role. The conservative piece of the relativistic correction only slightly changes the shape of trajectories in the phase space diagram (Sec. IV), where the gravitational radiation reaction tends to break the pair. It is also possible for resonant crossing to happen, where two or more resonant conditions are approximately satisfied, so that the system jumps from one resonance to another. If resonances start to overlap, this can lead to chaos [1]. We do not consider such cases here.

As the resonant pair spirals sufficiently close to the massive black hole, the gravitational radiation reaction becomes stronger than the disk force, and the resonant locking breaks down. In this case, the inner object merges with the massive black hole first, while its orbit is still influenced by the gravitational field of the outer object. We have analyzed the effect of such scenario in a separate study [22], where we show that the impact on the waveform of the inner object is possibly detectable by LISA, depending on the breaking radius of the pair. In fact, the tidal resonance effect studied there can be viewed as a “failed” capture of the relativistic mean motion resonance proposed here.

The paper is organized as follows. In Sec. II we derive an effective Hamiltonian describing the orbital dynamics near resonance in GR. We ignore any astrophysical effects and focus solely on the relativistic corrections. This effective Hamiltonian will be important in understanding the dynamics of bodies near mean motion resonance in the strong-gravity regime. Sec. III discusses an example of mean motion resonance: two point masses moving in the equatorial plane around a nonspinning black hole, with the inner orbit circular and the outer eccentric. From the level curves of the effective Hamiltonian, we can identify the resonant and nonresonant regimes of the phase space. In Sec. IV we present an effective Hamiltonian describing the orbital dynamics near resonance in post-Newtonian theory using Poincaré variables and compare it to its fully relativistic counterpart. Section V shows the results of a numerical study in which we evolve two stellar-mass black holes orbiting within the disk around a supermassive black hole using the N-body code REBOUND and including disk effects and relativistic corrections to the conservative and dissipative orbital evolution to leading post-Newtonian order. We study the capture into and breaking of resonance. Section VI summarizes the result and highlights some open issues.

Throughout this work we adopt geometric units by setting $c = G = 1$.

II. RELATIVISTIC HAMILTONIAN FORMALISM

We shall first consider the case that the interacting point masses are close to a massive black hole. In this fully relativistic regime, we can adopt black hole perturbation theory, where the point masses and the gravitational fields that they generate can be treated as perturbations of the spacetime of the massive black hole. A large body of literature has been devoted to the study of a single point mass moving in a large black hole’s spacetime under the influence of its own radiation reaction (the “self-force” problem), which is relevant for understanding the orbital evolution of EMRIs for LISA detection.² Here we place multiple point masses in the same background, so that their mutual gravitational interaction is also important. In addition to possible astrophysical applications, it is also theoretically interesting to explore multi-body effects in the strong-gravity regime.

A. Two-body Hamiltonian in Kerr background

The Hamiltonian of a single point mass moving in a curved background spacetime can be written as

$$\mathcal{H} = \frac{1}{2\mu} g_{\alpha\beta} p^\alpha p^\beta. \quad (2.1)$$

²Two nice review articles on this subject are [23,24].

With the set of canonical variables (x^β, p_β) and the above Hamiltonian, one can derive the Hamilton equation of motion for this point mass³:

$$\frac{dx^\beta}{d\tau} = \frac{\partial \mathcal{H}}{\partial p_\beta} = p^\beta, \quad \frac{dp_\beta}{d\tau} = -\frac{\partial \mathcal{H}}{\partial x^\beta}, \quad (2.2)$$

with τ being the proper time of the point mass. If the background spacetime is Kerr, four conserved quantities can be obtained from the equations of motion, and the orbital motion becomes separable:

$$\begin{aligned} \frac{d\theta}{d\lambda_m} &= \sqrt{Q - \cos^2\theta[a^2(\alpha^2 - E^2) + L_z^2/\sin^2\theta]}, \\ \frac{dr}{d\lambda_m} &= \sqrt{[E(r^2 + a^2) - L_z a]^2 - \Delta[r^2 + (L_z - aE)^2 + Q]}, \\ \frac{d\phi}{d\lambda_m} &= -\left(aE - \frac{L_z}{\sin^2\theta}\right) + \frac{a}{\Delta}[E(r^2 + a^2) - aL_z], \\ \frac{dt}{d\lambda_m} &= -a(aE\sin^2\theta - L_z) + \frac{r^2 + a^2}{\Delta}[E(r^2 + a^2) - L_z a]. \end{aligned} \quad (2.3)$$

where M , a are the mass and spin of the Kerr black hole, E , Q , L_z are the point mass energy, Carter's constant and angular momentum along the symmetry axis, respectively. Δ is defined as $r^2 - 2Mr + a^2$ and Mino time λ_m is related to proper time by $d/d\lambda_m = (r^2 + a^2 \cos^2\theta)d/d\tau$.

The stellar-mass objects of interest in this study are (of course) not point particles. If they carry nonzero spin, quadrupole moments and other higher order moments, additional couplings with the background curvature are expected. These additional complexities may be neglected if the stellar-mass object is a Schwarzschild black hole and its size is much smaller than the background radius of curvature. However, even in the point mass limit, in principle one should take into account the interaction of the object with its own gravitational field. This is known as the gravitational self-force. In order to derive the conserved dynamics of a point mass under the influence of the conservative piece of the self-force, one can decompose the metric as $g_{\alpha\beta} = g_{\alpha\beta}^{\text{Kerr}} + h_{\alpha\beta}$ [23], with the metric perturbation given by

$$h_{\alpha\beta}(x) = \mu \int d\tau' G_{\alpha\beta\rho\sigma}(x; x') u'^\rho u'^\sigma. \quad (2.4)$$

Here u is the four velocity of the particle and G is the half retarded, half advance Green function in Kerr spacetime [25,26]:

³For simplicity we have taken the rest mass to be $\mu = 1$.

$$G = \frac{1}{2}(G_{\text{ret}} + G_{\text{adv}}), \quad (2.5)$$

which is symmetric under time reversal operation ($t \rightarrow -t$). This metric perturbation $h_{\alpha\beta}$ has a diverging part, and one has to subtract a singular piece. The detailed procedure, known as *regularization*, is nicely explained in [27].

In principle as we Fourier decompose the metric perturbation generated by the point masses, we shall obtain an additional perturbative Hamiltonian with various Fourier harmonics (i.e., Eq. (2.7) and Eq. (2.8)). This perturbative Hamiltonian should contain a summation of contributions from the conservative self-force and mutual interactions of the stellar-mass objects.⁴ We are focusing on the resonance due to the mutual gravitational interaction in this study. The resonances due to self-interactions are independent of the other object and can be analyzed in a standard EMRI framework with a single object.⁵ We write the total Hamiltonian of two interacting bodies as

$$\begin{aligned} \mathcal{H} &= \frac{\mu}{2} g_{\alpha\beta}^{\text{Kerr}}(x) u^\alpha u^\beta + \frac{\mu}{2} g_{\alpha\beta}^{\text{Kerr}}(\underline{x}) \underline{u}^\alpha \underline{u}^\beta \\ &\quad + \frac{\mu}{2} \underline{h}_{\alpha\beta}(x) u^\alpha u^\beta + \frac{\mu}{2} h_{\alpha\beta}(\underline{x}) \underline{u}^\alpha \underline{u}^\beta \\ &=: \mathcal{H}_0 + \epsilon \mathcal{H}_{\text{int}} \end{aligned} \quad (2.6)$$

where \mathcal{H}_0 is the unperturbed Hamiltonian in the first line, \mathcal{H}_{int} is the perturbation described in the second line and ϵ is a book-keeping index for the perturbative Hamiltonian. The x , u are the position and velocity of the inner point mass, and \underline{x} , \underline{u} are those of the outer point mass. The metric perturbation h , \underline{h} can be obtained from Eq. (2.4) by plugging in the worldlines of the inner and outer point masses, respectively.

It is important to note that, at any given time, the inner object is only influenced by the part of outer object's worldline within the future and past lightcone of the inner object, and vice versa (cf. Fig. 1). This means that $\underline{h}_{\alpha\beta}(x)/h_{\alpha\beta}(\underline{x})$ is in principle independent of the outer/inner object's motion at time t , as they are causally disconnected. However, it turns out that it is still possible to write $\underline{h}_{\alpha\beta}(x)/h_{\alpha\beta}(\underline{x})$ as functions of \underline{x}/x at any given time. This is because to the leading order in mass ratios

⁴Any dissipative force, including the dissipative part of the self force, will change the system's "conserved" quantities such as energy and angular momentum. These changes typically do not alter the structure of the resonances, but do affect the capture probability into certain resonance (see e.g., [28]). For the analytic results in this paper, we therefore ignore any dissipation. However, in our numerical study in Sec. V we include dissipative effects.

⁵These resonances due to the self-interaction may affect the sustained transient resonance described in [29] for a single EMRI object.

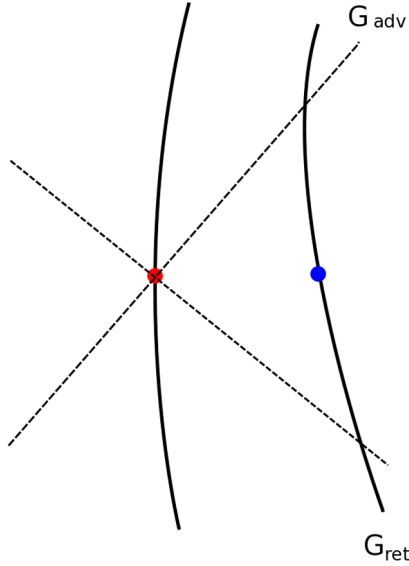


FIG. 1. Illustration of the worldlines of two point masses moving under the influence of a background black hole and mutual gravitational interaction. With the conservative Hamiltonian, the motion of one point mass is only affected by the portion of the other point mass's worldline lying in the first mass's future and past lightcone.

($\eta := \mu/M$, $\underline{\eta} := \underline{\mu}/M$), Eq. (2.4) only depends on the unperturbed, geodesic orbit of the point mass that sources the gravitational field.⁶ As the geodesic orbit is deterministic, specifying the position and momentum at any instant in time determines the whole worldline, including the parts that extend to the other point mass's past and future lightcones.

B. Canonical transformations

To analyze this problem in detail, we first separate the average adiabatic, the resonant and the nonresonant oscillatory terms in the Hamiltonian \mathcal{H} using action-angle variables $\{q, J\}$, $\{\underline{q}, \underline{J}\}$. The derivation that follows is rather general. In particular, it does not rely on the explicit form of the interaction Hamiltonian in Eq. (2.6), to which we return in the next section.

As the generalized angles q, \underline{q} have a period of 2π , the perturbed Hamiltonian can be simply decomposed as a Fourier series ($j = r, \theta, \phi$):

$$\mathcal{H}_{\text{int}} = \sum_{n_j, \underline{n}_j} H_{n_j, \underline{n}_j}(J, \underline{J}) e^{in_j q_j + i\underline{n}_j \underline{q}_j}, \quad (2.7)$$

with the Fourier coefficients given by

⁶Similar observations have been made for computing the leading order gravitational self-force of EMRIs.

$$H_{n_j, \underline{n}_j} = \frac{1}{(2\pi)^6} \int d^3 q_j d^3 \underline{q}_j \frac{\mu}{2} h_{\alpha\beta}(x; \underline{x}) u^\alpha u^\beta e^{-in_j q_j - i\underline{n}_j \underline{q}_j} + \frac{1}{(2\pi)^6} \int d^3 q_j d^3 \underline{q}_j \frac{\mu}{2} h_{\alpha\beta}(\underline{x}; x) \underline{u}^\alpha \underline{u}^\beta e^{-in_j q_j - i\underline{n}_j \underline{q}_j}. \quad (2.8)$$

Mean motion resonance may happen if a certain combination of q, \underline{q} , specifically $n_j q_j + \underline{n}_j \underline{q}_j$ with n_j and \underline{n}_j being integer, becomes a slowly varying quantity.⁷ In other words, when $n_j \omega_j + \underline{n}_j \underline{\omega}_j \approx 0$ is satisfied, with $\omega_j, \underline{\omega}_j$ being the frequencies of motion in r, θ, ϕ directions. Using this observation, the interaction Hamiltonian can be separated into an average adiabatic term, resonant terms and nonresonant oscillating terms:

$$\mathcal{H}_{\text{int}} = \bar{H}(J, \underline{J}) + \sum_k H_{kN_j, k\underline{N}_j}(J, \underline{J}) e^{ikN_j q_j + ik\underline{N}_j \underline{q}_j} + \sum_{n_j, \underline{n}_j \in R} H_{n_j, \underline{n}_j}(J, \underline{J}) e^{in_j q_j + i\underline{n}_j \underline{q}_j}, \quad (2.9)$$

where on resonance $n_j = N_j$, $\underline{n}_j = \underline{N}_j$, k is a nonzero integer and R is the set of all nonresonant 6-tuples: $\{(n_j, \underline{n}_j) \in \mathbb{Z} | (n_j, \underline{n}_j) \neq k(N_j, \underline{N}_j) \forall k \in \mathbb{Z}^\neq\}$. While the Hamiltonian nicely separates, the equations of motion for the action-angle variables couple oscillatory and resonant terms:

$$\begin{aligned} \frac{dq_i}{d\tau} &= \frac{\partial \mathcal{H}}{\partial J^i} \\ &= \Omega_i + \epsilon \frac{\partial \bar{H}(J, \underline{J})}{\partial J^i} + \epsilon \sum_k \frac{\partial H_{kN_j, k\underline{N}_j}}{\partial J^i} e^{ikN_j q_j + ik\underline{N}_j \underline{q}_j} \\ &\quad + \epsilon \sum_{n_j, \underline{n}_j \in R} \frac{\partial H_{n_j, \underline{n}_j}}{\partial J^i} e^{in_j q_j + i\underline{n}_j \underline{q}_j} \end{aligned} \quad (2.10)$$

$$\begin{aligned} \frac{dJ_i}{d\tau} &= -\frac{\partial \mathcal{H}}{\partial q^i} \\ &= -i\epsilon \sum_k k N_j H_{kN_j, k\underline{N}_j} e^{ikN_j q_j + ik\underline{N}_j \underline{q}_j}, \end{aligned} \quad (2.11)$$

where $\Omega_i := \partial \mathcal{H}_0 / \partial J^i$ and analogous equations hold for $\underline{q}_j, \underline{J}_i$. We introduce a change of variables to eliminate the dependence on the rapidly oscillating nonresonant terms to order ϵ following techniques in [30]. This change of variables is known as a ‘‘near-identity’’ transformation because for $\epsilon = 0$ this reduces to the identity transformation:

$$\tilde{q}_i(\vec{q}, \vec{J}, \vec{\underline{q}}, \vec{\underline{J}}) = q_i + \epsilon L_i(\vec{q}, \vec{J}, \vec{\underline{q}}, \vec{\underline{J}}) + \mathcal{O}(\epsilon^2) \quad (2.12)$$

⁷The Einstein summation rule has been applied, so that the explicit summation symbol is abbreviated.

$$\tilde{J}_i(\vec{q}, \vec{J}, \vec{q}, \vec{J}) = J_i + \epsilon T_i(\vec{q}, \vec{J}, \vec{q}, \vec{J}) + \mathcal{O}(\epsilon^2) \quad (2.13)$$

where

$$L_i = \bar{L}_i(\vec{J}, \vec{J}) + i \sum_{n_j, \underline{n}_j \in \mathbb{R}} \left[\frac{1}{n_j \Omega_j + \underline{n}_j \underline{\Omega}_j} \right] \frac{\partial H_{n_j, \underline{n}_j}}{\partial \tilde{J}^i} e^{in_j q_j + i \underline{n}_j \underline{q}_j} \quad (2.14)$$

$$T_i = \bar{T}_i(\vec{J}, \vec{J}) + i \sum_{n_j, \underline{n}_j \in \mathbb{R}} \left[\frac{n_i}{n_j \Omega_j + \underline{n}_j \underline{\Omega}_j} \right] H_{n_j, \underline{n}_j} e^{in_j q_j + i \underline{n}_j \underline{q}_j}, \quad (2.15)$$

with \bar{L}_i and \bar{T}_i arbitrary functions of J_i and \underline{J}_i . The underlined variables are analogously transformed. The freedom in \bar{L}_i and \bar{T}_i can be used to further simplify the equations, which may be convenient as one considers higher orders in ϵ ; for the calculation at hand, their behavior is irrelevant. The new variables now satisfy:

$$\frac{d\tilde{q}_i}{d\tau} = \Omega_i + \epsilon \frac{\partial \bar{H}}{\partial \tilde{J}^i} + \epsilon \sum_k \frac{\partial H_{k\mathbb{N}, k\mathbb{N}}}{\partial \tilde{J}^i} e^{ikN_j \tilde{q}_j + ik\underline{N}_j \tilde{q}_j} + \mathcal{O}(\epsilon^2), \quad (2.16)$$

$$\frac{d\tilde{J}_i}{d\tau} = -i\epsilon \sum_k k N_i H_{k\mathbb{N}, k\mathbb{N}} e^{ikN_j \tilde{q}_j + ik\underline{N}_j \tilde{q}_j} + \mathcal{O}(\epsilon^2), \quad (2.17)$$

where the nonresonant terms now decouple and do not contribute to the secular evolution of $\{\tilde{q}_i, \tilde{J}_i\}$ near resonance. Similar transformations and resulting equations hold for $\{\tilde{q}_i, \tilde{J}_i\}$.

In order to summarize the above equations of motion into one that is only controlled by the resonant d.o.f., we define

$$Q(\lambda) := \sum_i N_i \tilde{q}_i \left(\int \Gamma_i d\lambda \right) + \sum_i \underline{N}_i \tilde{q}_i \left(\int \underline{\Gamma}_i d\lambda \right), \quad (2.18)$$

with $\Gamma_i := \omega_i/\Omega_i$, $\underline{\Gamma}_i := \underline{\omega}_i/\underline{\Omega}_i$. Similar to Ω , $\underline{\Omega}$, the functional dependence of ω , $\underline{\omega}$ on J , \underline{J} can be obtained from the geodesic motion. While the action-angle variables depend only on their local proper time, physically λ plays the role of the coordinate time, such that the angles in Eq. (2.18) can add up with the same λ . With the presence of mutual gravitational interaction and near resonance, we can further define a *slow time* $\hat{\lambda} := \epsilon\lambda$. So that the equations of motion become

$$\begin{aligned} \frac{dQ}{d\hat{\lambda}} &= \frac{1}{\epsilon} \sum_i (N_i \omega_i + \underline{N}_i \underline{\omega}_i) + \sum_i \Gamma_i N_i \frac{\partial \bar{H}}{\partial \tilde{J}^i} \\ &+ \sum_i \underline{\Gamma}_i \underline{N}_i \frac{\partial \bar{H}}{\partial \tilde{J}^i} + \sum_{i,k} \Gamma_i N_i \frac{\partial H_{k\mathbb{N}, k\mathbb{N}}}{\partial J_i} e^{ikQ} \\ &+ \sum_i \underline{\Gamma}_i \underline{N}_i \sum_k \frac{\partial H_{k\mathbb{N}, k\mathbb{N}}}{\partial \underline{J}_i} e^{ikQ} + \mathcal{O}(\epsilon), \\ \frac{d\tilde{J}_i}{d\hat{\lambda}} &= -i \sum_k k \Gamma_i N_i H_{k\mathbb{N}, k\mathbb{N}} e^{ikQ} + \mathcal{O}(\epsilon), \\ \frac{d\tilde{J}_i}{d\hat{\lambda}} &= -i \sum_k k \underline{\Gamma}_i \underline{N}_i H_{k\mathbb{N}, k\mathbb{N}} e^{ikQ} + \mathcal{O}(\epsilon). \end{aligned} \quad (2.19)$$

Here, we focus on the system of equations for Q , \tilde{J}_i , \tilde{J}_i ; the other phases not encoded in Q can be recovered by direct integration after having solved for Q , \tilde{J}_i , \tilde{J}_i . We denote $\Delta\omega := \frac{1}{\epsilon} \sum_i (N_i \omega_i + \underline{N}_i \underline{\omega}_i)$ and note that resonance is only present if this quantity is proportional to the mass ratio between the point masses and the primary massive black hole. This observation is similar to the analysis of mean motion resonance in the Newtonian limit [1]. In other words, in order to find resonance, this term is comparable to the terms involving $H_{k\mathbb{N}, k\mathbb{N}}$, which is also proportional to the mass ratio. In principle with the initial condition defined, Eq. (2.19) is able to predict the system evolution at any later time (provided of course all the above approximations still hold).

To understand the long-term dynamics of the mean motion resonance, it is often convenient to use a simplified, effective Hamiltonian and study its level sets. However, based on Eq. (2.19), it is not clear whether it is possible to write down an effective Hamiltonian for Q and its conjugate momentum Θ in the most general setting. We can nevertheless restrict to the parameter regime where Γ_i , $\underline{\Gamma}_i$ are approximately constants. As they are functions of action variables, they are approximately constants whenever resonant motion only induces small variation on the conserved quantities, e.g., the cases with eccentricity being small. We will assume this is the case. We also note that the terms coming from the adiabatic part of the Hamiltonian, while generically important to understand the dynamics of the system, can be regarded as constants near resonance and we shall drop them from hereon after.

Under these approximations, let us expand $\Delta\omega$:

$$\Delta\omega = \Delta\omega \Big|_{\Theta=0} + \frac{\partial \Delta\omega}{\partial \Theta} \Big|_{\Theta=0} + \mathcal{O}(\epsilon) \quad (2.20)$$

and rewrite the first line in Eq. (2.19) as

$$\begin{aligned} \frac{dQ}{d\lambda} &\approx \alpha + 2\beta\Theta + \sum_{i,k} \Gamma_i N_i \frac{\partial H_{k\mathbf{N},k\mathbf{N}}}{\partial J_i} e^{ikQ} \\ &+ \sum_i \Gamma_i N_i \sum_k \frac{\partial H_{k\mathbf{N},k\mathbf{N}}}{\partial J_i} e^{ikQ} + \text{H.c.}, \end{aligned} \quad (2.21)$$

with

$$\begin{aligned} \alpha &:= \Delta\omega|_{\Theta=0}, \\ \beta &:= \frac{1}{2} \frac{\partial \Delta\omega}{\partial \Theta} \Big|_{\Theta=0}. \end{aligned} \quad (2.22)$$

Given that $\Delta\omega = \Delta\omega(\Theta, \hat{\lambda})$, the associated Hamiltonian is nonlinear in Θ and this allows for the mean motion resonance to occur. If $\Delta\omega$ was independent of Θ , only transient resonance would be possible. We make the following identification with the action variables:

$$\begin{aligned} N_i \Gamma_i \Theta + \Theta_i &= \tilde{J}_i, \\ \underline{N}_i \Gamma_i \Theta + \underline{\Theta}_i &= \tilde{J}_i, \end{aligned} \quad (2.23)$$

with $\Theta_i, \underline{\Theta}_i$ being constants, so that Eq. (2.21) and Eq. (2.19) are compatible with the effective Hamiltonian

$$\begin{aligned} H_{\text{eff}} &= \alpha\Theta + \beta\Theta^2 + \sum_k H_{k\mathbf{N},k\mathbf{N}} e^{ikQ} \\ &= \alpha\Theta + \beta\Theta^2 + 2 \sum_{k \geq 1} \text{Re}(H_{k\mathbf{N},k\mathbf{N}}) \cos kQ \\ &\quad - 2 \sum_{k \geq 1} \text{Im}(H_{k\mathbf{N},k\mathbf{N}}) \sin kQ. \end{aligned} \quad (2.24)$$

In order to study the resonance dynamics described by this effective Hamiltonian, it is necessary to explicitly write down the dependence of $H_{\mathbf{N},\mathbf{N}}$ on Θ . As we shall see in Sec. IV, in the Newtonian limit, the interaction Hamiltonian scales as $\Theta^{1/2}$ for the lowest order resonances (that is, those with $n_r, n_z = \pm 1$), and $\Theta^{N/2}$ with $N \geq 1$ in general. In the relativistic regime, we shall assume that similar power-law behavior still holds when Θ is small. For example, for the resonance considered in Sec. III, it is natural to expect that $\Theta \propto \underline{J}_r \propto \underline{e}^2$, with e being the eccentricity, and $H_{\mathbf{N},\mathbf{N}} \propto \underline{e}$ when $\underline{e} \ll 1$. As a result, we expect $H_{\mathbf{N},\mathbf{N}} \propto \Theta^{1/2}$.

Remark. The above canonical transformations from the action-angle variables to the final $\{Q, \Theta\}$ can be summarized as follows:

$$\{q_i, J_i, \underline{q}_i, \underline{J}_i\} \xrightarrow{F_1} \{\tilde{q}_i, \tilde{J}_i, \tilde{\underline{q}}_i, \tilde{\underline{J}}_i\} \xrightarrow{F_2} \{Q, \Theta\} \quad (2.25)$$

where F_1 and F_2 are generating functions, given by:

$$\begin{aligned} F_1(q, \tilde{J}, q, \tilde{J}) &= \sum_{i=1}^3 (q_i \tilde{J}_i + \underline{q}_i \tilde{J}_i) + \epsilon F_1^{(1)}(q, \tilde{J}, q, \tilde{J}) \\ F_2(\tilde{q}, \Theta) &= \sum_k (N_k \tilde{q}_k + \underline{N}_k \tilde{\underline{q}}_k) \Theta + \dots \end{aligned} \quad (2.26)$$

with the dots indicating (irrelevant) nonresonant terms and L_i and T_i in Eqs. (2.14)–(2.15) are related to $F^{(1)}$ through its derivatives

$$L_i = \frac{\partial F^{(1)}}{\partial \tilde{J}^i} \quad (2.27)$$

$$T_i = -\frac{\partial F^{(1)}}{\partial q^i}. \quad (2.28)$$

Canonical transformations of course do not reduce the size of phase space, the fact that we go from 2×6 to only 1×2 variables is due to the fact that we have decoupled the oscillatory pieces from the resonant ones and we focus only on the behavior of the resonant terms.

III. RESONANCE EXAMPLE

In this section, we illustrate how to compute the resonance Hamiltonian, by explicitly evaluating an example of a $n_\phi : n_r : n_\phi = 2 : 1 : -2$ resonance with system parameters given in Table I.

A. General prescription for calculating the interaction Hamiltonian

In Sec. II we have derived the effective Hamiltonian of two point masses undergoing relativistic mean motion resonance, as shown in Eq. (2.24). The key part of this effective Hamiltonian is the interaction part $H_{\mathbf{N},\mathbf{N}}$, which requires Fourier transforming the metric perturbation generated by a moving point mass. Let us consider the part of the integral in Eq. (2.8),

$$h_{\alpha\beta}^N(\underline{x}) := \frac{1}{(2\pi)^3} \int d^3\mathbf{q} h_{\alpha\beta}(\underline{x}; x) e^{-i\mathbf{N}\cdot\mathbf{q}}, \quad (3.1)$$

with the inverse decomposition given by

$$h_{\alpha\beta}(\underline{x}; x) = \sum_{\mathbf{N}} h_{\alpha\beta}^N(\underline{x}) e^{i\mathbf{N}\cdot\mathbf{q}}. \quad (3.2)$$

TABLE I. Orbital parameters for the resonant, equatorial orbit studied in Sec. III. This orbit corresponds to the case with $2\underline{\omega}_\phi + \underline{\omega}_r - 2\underline{\omega}_\phi \approx 0$.

\underline{r}_{\min}/M	\underline{r}_{\max}/M	r/M	$\underline{\omega}_\phi M$	$\underline{\omega}_r M$	$\omega_\phi M$
25	30	21.53	6.94×10^{-3}	6.13×10^{-3}	10^{-2}

For a fixed worldline of the source, the metric perturbation at different \underline{t} undergoes periodic oscillations, as the source is periodic. In other words, we can also write

$$h_{\alpha\beta}(\underline{x}; x) = \sum_{\mathbf{N}} h_{\omega\mathbf{N};\alpha,\beta}(\underline{L}, \underline{\theta}, \underline{\phi}) e^{-i\omega\cdot\mathbf{N}\underline{t}} \quad (3.3)$$

with $\omega = (\omega_r, \omega_\theta, \omega_\phi)$, and the inverse transformation

$$h_{\omega\mathbf{N};\alpha,\beta}(\underline{L}, \underline{\theta}, \underline{\phi}) = \lim_{T \rightarrow \infty} \frac{1}{T} \int_0^T d\underline{t} h_{\alpha\beta}(\underline{x}; x) e^{i\omega\cdot\mathbf{N}\underline{t}}. \quad (3.4)$$

Now the time translational invariance implies that (with $x_0 = \{t_0, r_0, \theta_0, \phi_0\}$, $\underline{x} = \{\underline{L}, \underline{r}, \underline{\theta}, \underline{\phi}\}$)

$$h_{\alpha\beta}(\underline{L} + \underline{t}, \underline{r}, \underline{\theta}, \underline{\phi}; x_0) = h_{\alpha\beta}(\underline{x}; t_0 - \underline{t}, r_0, \theta_0, \phi_0). \quad (3.5)$$

As a result, Eq. (3.4) can be rewritten as

$$\begin{aligned} h_{\omega\mathbf{N};\alpha,\beta}(\underline{L}, \underline{\theta}, \underline{\phi}) &= \lim_{T \rightarrow \infty} \frac{1}{T} \int_0^T dt h_{\alpha\beta}(\underline{x}; x)|_{\underline{t}=0} e^{-i\omega\cdot\mathbf{N}t} \\ &= \lim_{T \rightarrow \infty} \frac{1}{T} \int_0^T dt \sum_{\mathbf{N}'} h_{\alpha\beta}^{\mathbf{N}'}(\underline{x})|_{\underline{t}=0} e^{i\mathbf{N}'\cdot\mathbf{q}} e^{-i\omega\cdot\mathbf{N}t}. \end{aligned} \quad (3.6)$$

The above expression can be recast in a simpler form:

$$h_{\omega\mathbf{N};\alpha,\beta} = M_{\mathbf{N},\mathbf{N}'} h_{\alpha\beta}^{\mathbf{N}'} \quad (3.7)$$

or

$$h_{\alpha\beta}^{\mathbf{N}'} = M_{\mathbf{N},\mathbf{N}'}^{-1} h_{\omega\mathbf{N};\alpha,\beta} \quad (3.8)$$

with $[\mathbf{\Omega} = (\Omega_r, \Omega_\theta, \Omega_\phi)]$

$$M_{\mathbf{N},\mathbf{N}'} := \lim_{T \rightarrow \infty} \frac{1}{T} \int_0^T d\tau u^t e^{i\mathbf{N}'\cdot\mathbf{\Omega}\tau} e^{-i\omega\cdot\mathbf{N}t(\tau)}. \quad (3.9)$$

In reality, $h_{\omega\mathbf{N};\alpha,\beta}$ can be obtained from a frequency-domain code that computes the metric perturbation, or reconstructed from master variables (such as Teukolsky variables or master variables in the Regge-Wheeler equation) in a frequency-domain code. Equation (3.8) then enables us to compute $H_{\mathbf{N},\mathbf{N}'}$ from $h_{\omega\mathbf{N};\alpha,\beta}$.

B. Frequency-domain Schwarzschild metric perturbation

For simplicity, let us illustrate relativistic mean motion resonance in the Schwarzschild spacetime, with two point masses moving along equatorial orbits. At the leading order, i.e., in the geodesic limit, we assume that the inner point mass moves along a circular orbit and the outer point mass moves along an eccentric orbit. We assume that the system is close to the resonance such that

$$2\underline{\omega}_\phi + \underline{\omega}_r - 2\underline{\omega}_\theta \approx 0. \quad (3.10)$$

In other words, we shall consider the dynamical variable $Q = 2q_\phi + q_r - 2q_\theta$. This can be achieved with a range of possibilities, and we will adopt the values shown in Table I for constructing the point mass trajectory. Notice that in the Newtonian limit ω_ϕ becomes similar to ω_r , so that the $n_\phi : n_r : n_\theta = 2 : 1 : -2$ resonance considered here naturally becomes the 3:2 outer resonance well studied in planetary systems.⁸

In the frequency domain, the metric perturbation of Schwarzschild black holes, decomposed as spherical harmonics, can be written as (following the convention in [32])

$$\begin{aligned} \mathbf{h}_{\ell m} &= f(r) H_{0\ell m}(r) \mathbf{a}_{\ell m}^{(0)} + H_{1\ell m}(r) \mathbf{a}_{\ell m}^{(1)} \\ &\quad + \frac{1}{f(r)} H_{2\ell m}(r) \mathbf{a}_{\ell m} + h_{0\ell m}^{(e)}(r) \mathbf{b}_{\ell m}^{(0)} + h_{1\ell m}^{(e)}(r) \mathbf{b}_{\ell m} \\ &\quad + \frac{r^2}{2} G_{\ell m}(r) \mathbf{f}_{\ell m} + r^2 \left[K_{\ell m}(r) - \frac{\ell(\ell+1)}{2} G_{\ell m}(r) \right] \mathbf{g}_{\ell m} \\ &\quad - h_{0\ell m}(r) \mathbf{c}_{\ell m}^{(0)} - h_{1\ell m}(r) \mathbf{c}_{\ell m} + i h_{2\ell m}(r) \mathbf{d}_{\ell m}, \end{aligned} \quad (3.11)$$

where $f(r) = 1 - 2M/r$, the tensor components $\mathbf{a}_{\ell m}^{(0)}$, $\mathbf{a}_{\ell m}^{(1)}$, $\mathbf{a}_{\ell m}$, $\mathbf{b}_{\ell m}^{(0)}$, $\mathbf{b}_{\ell m}$, $\mathbf{f}_{\ell m}$, $\mathbf{g}_{\ell m}$, $\mathbf{c}_{\ell m}^{(0)}$, $\mathbf{c}_{\ell m}$, $\mathbf{d}_{\ell m}$ are given in Appendix A and the common time dependence factor $e^{-i\omega t}$ has been omitted. In the Regge-Wheeler gauge, the metric quantities $h_{0\ell m}^{(e)}(r)$, $h_{1\ell m}^{(e)}(r)$, $G_{\ell m}(r)$, $h_{2\ell m}(r)$ are set to be zero. The remaining metric quantities can be reconstructed by the odd and even parity master variables Ψ^o , Ψ^e , which are solutions of the master wave equations

$$[\partial_{r_*}^2 + \omega^2 - V^o(r)] \Psi^o = S^o(r), \quad (3.12)$$

and

$$[\partial_{r_*}^2 + \omega^2 - V^e(r)] \Psi^e = S^e(r), \quad (3.13)$$

with $dr_* = (1 - 2M/r)^{-1} dr$. Here the source terms S^o , S^e are explicitly given in [31]. For point masses these sources contain δ functions and their first derivatives, which are the origin of the kinks and the discontinuity in Ψ^e in Fig. 2.⁹ The potential terms are

⁸Here the *outer resonance* refers to a resonance with resonant Hamiltonian proportional to the eccentricity of the outer object to a certain power. Similarly an *inner resonance* corresponds to one with resonant Hamiltonian proportional to the eccentricity of the inner object to a certain power. Note these definitions apply only for leading-order resonances. Operationally when we see a $\underline{\omega}_r$ in the resonance condition, it is an outer resonance.

⁹Numerically we use a narrow Gaussian profile to approximate the δ function, so that the kinks and the discontinuity are not infinitely sharp in Fig. 2.

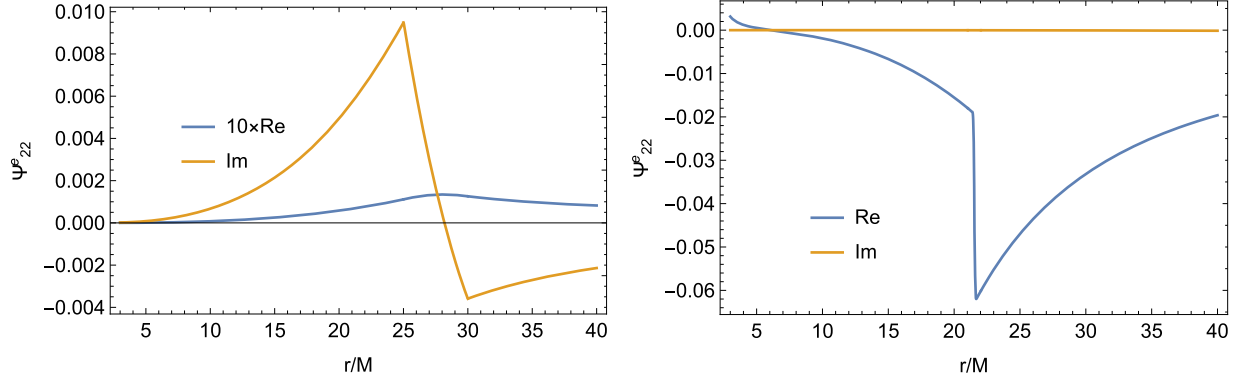


FIG. 2. The even parity master variable Ψ^e as a solution of the $\ell = 2, m = 2$ Master equation Eq. (3.13) with eccentric (Left panel) and circular (Right panel) source term as described in Table I. The frequency domain Master equations are solved at a fixed ω , in particular, $\omega = 2\omega_\phi + \omega_r = 2\omega_\phi$. For the eccentric case, the real part is significantly smaller than the imaginary part of Ψ^e and we have therefore multiplied the real part by a factor of 10 to see its behavior. For the circular case, the imaginary part is identically zero as the source term is entirely real (see [31] for details). The odd parity master variable Ψ^o is zero because of the parity symmetry and therefore not shown.

$$\begin{aligned}
 V^o(r) &= \left(1 - \frac{2M}{r}\right) \left(\frac{2(\lambda_l + 1)}{r^2} - \frac{6M}{r^3}\right), \\
 V^e(r) &= \left(1 - \frac{2M}{r}\right) \\
 &\quad \times \frac{2\lambda_l^2(\lambda_l + 1)r^3 + 6\lambda_l^2Mr^2 + 18\lambda_lM^2r + 18M^3}{r^3(r\lambda_l + 3)^2},
 \end{aligned} \tag{3.14}$$

with $\lambda_l = (\ell - 1)(\ell + 2)/2$. For the source trajectory considered here, the $\ell = 2, m = \pm 2$ piece of metric perturbation dominates. In addition, the odd-parity source terms are zero, such that the odd-parity metric perturbations are also zero. We numerically solve the even-parity master equation by applying ingoing boundary condition at horizon and outgoing boundary condition at infinity. The results for the trajectory described in Table I is shown in Fig. 2. The metric quantities are directly reconstructed based on the solutions of Ψ^e . The advanced solution may be obtained by imposing outgoing condition at horizon and ingoing solution at infinity.

C. Phase space

With the trajectory in Table I and the reconstructed metric perturbations, we can explicitly write down the effective Hamiltonian. For simplicity we assume that the masses of the resonant objects are the same $\mu = \mu'$, so that $\eta = \eta'$.

$$H_{\text{eff}} \approx \alpha\Theta - 0.032\eta\Theta^2 + 0.02\eta\sqrt{\Theta}(6\sin Q + 3.1\cos Q), \tag{3.15}$$

where this is an approximate expression as we have only kept the dominant $\ell = 2, m = \pm 2$ harmonics. The conjugate momentum is given by $\Theta = \Gamma_r J_r / \mu$ in this particular example. Next, we rescale the Hamiltonian by a factor

$10^{-2}\eta$, which is equivalent to rescaling the time. The new Hamiltonian is

$$H'_{\text{eff}} = \delta\Theta - 3.2\Theta^2 + 2\sqrt{\Theta}(6\sin Q + 3.1\cos Q) \tag{3.16}$$

with $\delta := \alpha/(0.01\eta)$. The phase space trajectories follow level curves of H'_{eff} and are shown in Fig. 3 in terms of (Θ, Q) . The topology of the phase space is completely determined by H'_{eff} and depends only upon the value of δ : There are cases where the phase space can be naturally divided into a “rotation” regime and a “libration” regime, and cases where there is only a rotation regime. The motion in the libration regime is trapped, which corresponds to the mean motion resonance considered here. Different libration regimes are equivalent to each other due to the $Q \rightarrow Q + 2\pi$ symmetry of the effective Hamiltonian.

For illustration purposes, we also define

$$X = \sqrt{2\Theta}\cos Q, \quad Y = \sqrt{2\Theta}\sin Q, \tag{3.17}$$

with the corresponding phase space trajectories shown in Fig. 4. The origin in these plots corresponds to zero eccentricity, and the distance from the origin is proportional to the eccentricity. The orbits in the rotation regime correspond to the cases that the resonance is broken.

In the effective Hamiltonian above we consider α/δ as constant. However, to properly account for the secular dynamics, we also need to consider the parametric modification of α/δ due to the secular change of the system’s energy, angular momentum, etc. When this is taken into account, the actual trajectories in phase space are not the closed trajectories in the (X, Y) phase plane shown in Fig. 4. Nonetheless, these level curves of the effective Hamiltonian are very useful as they serve as “guiding” trajectories for the evolution. In particular, from the trajectories it is clear that if one is near resonance so that the effective

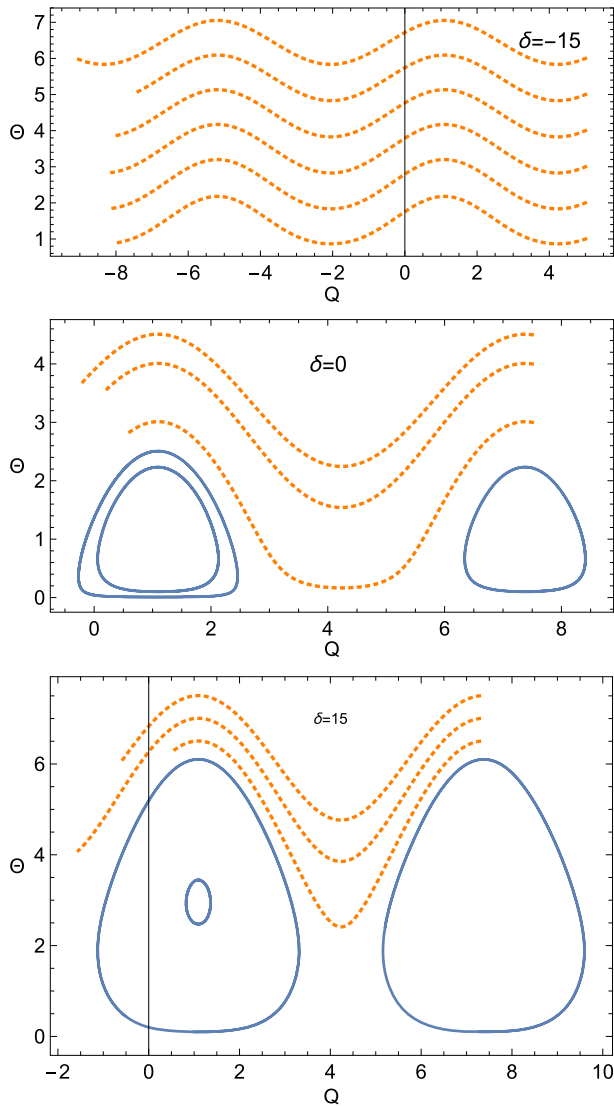


FIG. 3. The trajectories in phase space corresponding to the effective Hamiltonian described by Eq. (3.15). For both $\delta = 0$ and $\delta = 15$ cases, there are two regimes in the phase space: the libration regime (solid, blue lines) and the rotation regime (dashed, orange lines). There is only a rotation regime for $\delta = -15$.

Hamiltonian describes the evolution of the system, but not on resonance yet, and one has $\delta < 0$, a necessary (but not sufficient) condition for resonance to occur is that δ has to increase such that it becomes positive [1]. And vice versa, if δ is initially positive, $\dot{\delta}$ needs to be negative for resonance to occur. In addition, the action of an orbit, that is,

$$J = \oint \Theta dQ = \oint X dY, \quad (3.18)$$

is an adiabatic invariant of motion, and in this case is simply the area enclosed by a phase space trajectory in the (X, Y) plane. The action is not conserved when the orbits evolves close to the resonant critical curve/separatrix (as there the period of the motion becomes infinite). Therefore,

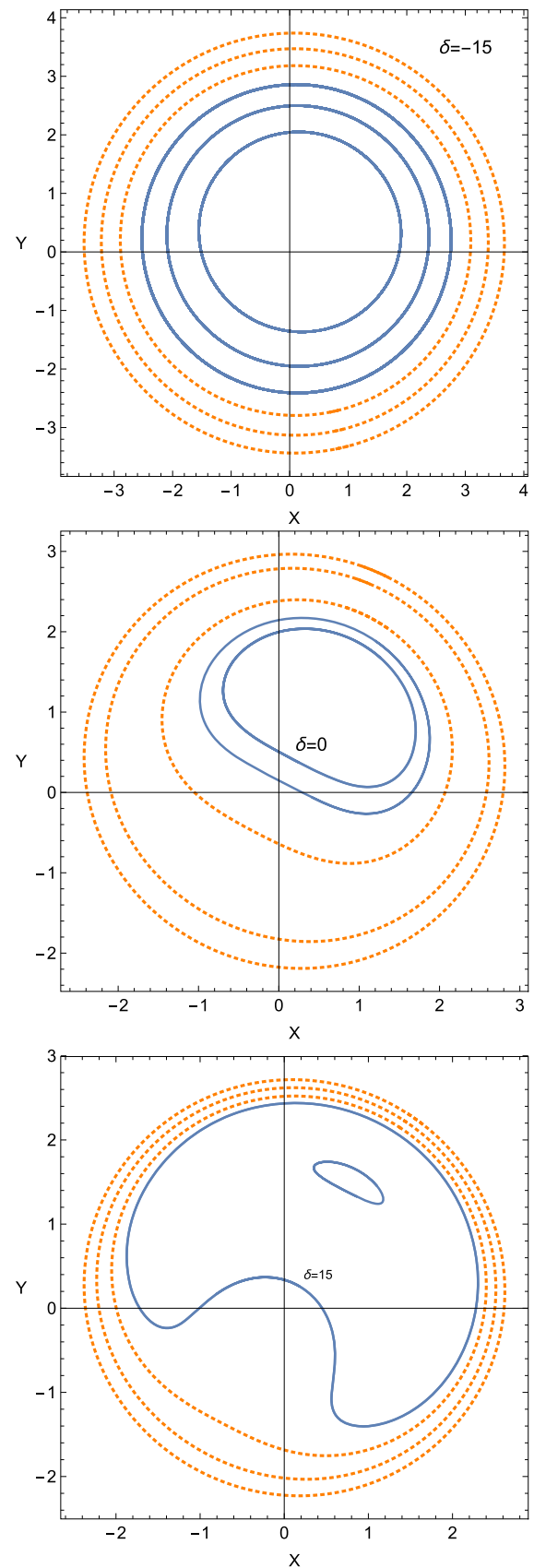


FIG. 4. Same phase space trajectories as in Fig. 3, although the canonical variables are chosen as in Eq. (3.17).

for guiding trajectories which remain away from the critical curve, adiabatic changes in δ preserve the area enclosed by the trajectory in the (X, Y) -plane, even as its center moves. After the critical curve has been crossed the action again becomes an approximate adiabatic invariant. Based on these considerations, one can qualitatively predict the possible outcomes of capture into resonance. For instance, consider conditions near resonance with $\delta < 0$, $\dot{\delta} > 0$ and with initial small eccentricity (in other words, the area enclosed by the guiding trajectory is small). As δ increases, the trajectory can stay in the circulation regime and “miss” the resonance or it can be captured into resonance. If capture occurs, the resulting eccentricity will be larger as the guiding trajectory will be off-center (see Fig. 4). Hence, for the effective Hamiltonian H'_{eff} , there is a significant change in the eccentricity due to capture into resonance. In realistic situations, we also need to take into account the dissipative forces that drive the orbital migration, which likely affect the resonance capture and evolution as well. This is seen in the numerical evolution of various resonances in Sec. V. In that section, we also discuss in more detail the dynamics near resonance accounting for the evolution of the orbital parameters due to dissipation.

IV. POST-NEWTONIAN HAMILTONIAN FORMALISM

In this section, we derive an effective post-Newtonian Hamiltonian to analyze the dynamics near mean motion resonance. We restrict ourselves to the case of two small bodies with masses μ and $\underline{\mu}$ orbiting the central massive object M in the equatorial plane.

The Hamiltonian of this system, which we denote by H to distinguish it from the relativistic Hamiltonian \mathcal{H} , can be written as:

$$H = H_1 + H_2 + H_{\text{int}} \quad (4.1)$$

where H_1 is the Hamiltonian of body μ , H_2 that of body $\underline{\mu}$ and H_{int} is the interaction Hamiltonian. To make the different Newtonian orders explicit, we will (partially) reinstate factors of c in this section, but the gravitational constant G is still set to one. To first post-Newtonian order H_1 is given by [33]

$$\begin{aligned} H_1 = & \frac{1}{2\mu} \left(p_r^2 + \frac{p_\phi^2}{r^2} \right) - \frac{\mu M}{r} \\ & + \frac{1}{c^2} \left[-\frac{1}{8\mu^3} \left(p_r^2 + \frac{p_\phi^2}{r^2} \right)^2 + \frac{\mu M^2}{2r} \right. \\ & \left. - \frac{3M}{2\mu r} \left(p_r^2 + \frac{p_\phi^2}{r^2} \right) \right] + \mathcal{O}\left(\frac{1}{c^4}\right) \end{aligned} \quad (4.2)$$

and similarly for the second body with the relevant quantities denoted with an underbar. We will return to

the explicit form of the interaction Hamiltonian, but first we will rewrite H_1 (and H_2) in terms of Poincaré variables. These variables are a linear combination of the standard action-angle variables associated to the coordinates r, ϕ and have been extremely valuable in the study of planetary dynamics.¹⁰ In order to perform the transformation to Poincaré variables, we first observe that ϕ is a cyclic coordinate so that p_ϕ is constant and make a canonical transformation to action-angle variables

$$J_r := \frac{1}{2\pi} \oint p_r dr \quad (4.3)$$

$$J_\phi := \frac{1}{2\pi} \oint p_\phi d\phi = p_\phi. \quad (4.4)$$

Using the fact that H_1 is conserved and denoting this constant H_1 by E (with $E < 0$ as we consider bound orbits), we write $p_r = p_r(r, E, p_\phi)$

$$\begin{aligned} p_r = & \pm \frac{\sqrt{-2\mu E}}{r} \sqrt{(r-r_-)(-r+r_+)} \\ & \pm \frac{1}{c^2} \frac{r}{2\sqrt{-2\mu E}} \frac{E^2 + \frac{8\mu M E}{r} + \frac{6\mu^2 M^2}{r^2}}{\sqrt{(r-r_-)(-r+r_+)}} + \mathcal{O}\left(\frac{1}{c^4}\right) \end{aligned} \quad (4.5)$$

with r_- and r_+ defined by the requirement that the Newtonian part of p_r vanishes

$$r_\pm = \frac{\mu M \pm \sqrt{\mu^2 M^2 + \frac{2p_\phi^2 E}{\mu}}}{-2E}. \quad (4.6)$$

Substituting Eq. (4.5) into the definition for J_r , and performing the relevant integrals (using standard contour integration), we obtain:

$$\begin{aligned} J_r = & -p_\phi + \frac{\mu^2 M}{\sqrt{-2\mu E}} \\ & + \frac{1}{c^2} \left[-\frac{15}{8} M \sqrt{-2\mu E} + 3 \frac{\mu^2 M^2}{p_\phi} \right] + \mathcal{O}\left(\frac{1}{c^4}\right). \end{aligned} \quad (4.7)$$

In principle, we should have taken into account that r_\pm is shifted by post-Newtonian corrections and therefore that the integration limits in Eq. (4.3) are also shifted and not simply r_\pm . A careful analysis of these “edge” contributions shows that their change is subdominant and we shall neglect these corrections. From the standard action-angle variables $\{q_r, q_\phi, J_r, J_\phi\}$, we perform a canonical transformation to the Poincaré variables

¹⁰Delauney variables—another frequently used set of variables in celestial mechanics—are yet another linear combination of the standard action-angle variables. However, these have the disadvantage that they are not well-defined for orbits with vanishing eccentricities.

$$\begin{aligned}\gamma &= q_r - q_\phi & \Gamma &= J_r \\ \lambda &= q_\phi & \Lambda &= J_r + J_\phi.\end{aligned}\quad (4.8)$$

The generating function of this transformation is

$$F = (q_r - q_\phi)\Gamma + q_\phi\Lambda. \quad (4.9)$$

After these canonical transformations, the Hamiltonian for the body with mass μ is

$$H_1 = -\frac{\mu^3 M^2}{2\Lambda^2} + \frac{1}{c^2} \frac{3\mu^5 M^4}{8\Lambda^4} \frac{5\Gamma + 3\Lambda}{\Gamma - \Lambda} + \mathcal{O}\left(\frac{1}{c^4}\right). \quad (4.10)$$

This Hamiltonian recovers the well-known post-Newtonian precession rate to first post-Newtonian order [33]:

$$\begin{aligned}\dot{\gamma} &= \frac{\partial H_1}{\partial \Gamma} = -\frac{3}{c^2} \frac{\mu^5 M^4}{\Lambda^3 (\Gamma - \Lambda)^2} + \mathcal{O}\left(\frac{1}{c^4}\right) = \omega_r - \omega_\phi \\ \dot{\lambda} &= \frac{\partial H_1}{\partial \Lambda} = \frac{\mu^3 M^2}{\Lambda^3} \\ &\quad - \frac{1}{c^2} \frac{3\mu^5 M^4}{2\Lambda^5} \frac{5\Gamma^2 - 4\Lambda\Gamma - 3\Lambda^2}{(\Gamma - \Lambda)^2} + \mathcal{O}\left(\frac{1}{c^4}\right) = \omega_\phi\end{aligned}$$

where

$$\omega_r = \frac{(-2E)^{3/2}}{\mu^{3/2} M} \left(1 + \frac{1}{c^2} \frac{15E}{4\mu}\right) + \mathcal{O}\left(\frac{1}{c^4}\right) \quad (4.11)$$

$$\omega_\phi = \frac{(-2E)^{3/2}}{\mu^{3/2} M} \left(1 + \frac{1}{c^2} \left(\frac{15E}{4\mu} + 3\frac{\mu^2 M^2}{p_\phi^2}\right)\right) + \mathcal{O}\left(\frac{1}{c^4}\right) \quad (4.12)$$

(see Eq. (345) in [33] after identifying ω_r with n and ω_ϕ with nK).

While this formalism allows us to investigate resonance behavior in a variety of circumstances, here we focus on a particular simple case: a first order exterior $j-1:j$ resonance (also known as an outer resonance), whereby the internal object μ completes $j-1$ cycles and the external object $\underline{\mu}$ completes j cycles before the system returns to its original state. We focus on first order resonances as lower order mean motion resonances are more important than higher order ones for the orbital dynamics of three-body systems.

The interaction Hamiltonian describes the gravitational interaction between the body with μ and that with $\underline{\mu}$. It contains terms that can be classified as short period, secular and resonant. The short period terms vanish after orbit

averaging and contribute negligible to the long term dynamics of the system. Therefore, for most purposes these short term terms can be ignored. The secular and resonant terms are both important for a complete understanding of the orbital dynamics. However, to understand the dynamics of the system near resonance, the resonant terms dominate so that we can consider the following simple form for the interaction Hamiltonian [1]

$$H_{\text{int}} = -f_d \frac{\mu \underline{\mu}^3 M}{\underline{\Lambda}^2} \sqrt{\frac{2\underline{\Gamma}}{\underline{\Lambda}}} \cos((1-j)\underline{\lambda} + j\lambda + \underline{\gamma}) + \mathcal{O}\left(\frac{1}{c^2}\right), \quad (4.13)$$

with f_d indicating the strength of the interaction. Although f_d is in principle a function of the ratio of the semimajor axes of the two orbiting bodies, its functional dependence is not relevant to the orbital dynamics and we will treat it as a constant [34].

The expressions so far are valid for any value of eccentricity. To further simplify the analysis, we expand the above Hamiltonian for small eccentricities following similar steps in [1]. In order to perform the small eccentricity expansions, we yet again make a canonical transformation:

$$\begin{aligned}\theta_1 &= (1-j)\underline{\lambda} + j\lambda + \gamma & \Theta_1 &= \Gamma \\ \theta_2 &= (1-j)\underline{\lambda} + j\lambda + \underline{\gamma} & \Theta_2 &= \underline{\Gamma} \\ \theta_3 &= \lambda & \Theta_3 &= \Lambda - j(\Gamma + \underline{\Gamma}) \\ \theta_4 &= \underline{\lambda} & \Theta_4 &= \underline{\Lambda} - (1-j)(\Gamma + \underline{\Gamma}).\end{aligned}\quad (4.14)$$

For an exterior resonance, the new coordinates θ_1 , θ_3 and θ_4 are all cyclic so that the associated momenta Θ_1 , Θ_3 and Θ_4 are constant. Therefore, the problem has effectively been reduced to a system with one d.o.f. described by $\{\theta_2, \Theta_2\}$. (For interior resonances, the story is very similar and the effective d.o.f. is described by $\{\theta_1, \Theta_1\}$.) By relating the momenta to the orbital elements, and in particular to the Newtonian eccentricity e , we find that $\Theta_1, \Theta_2 \sim \mathcal{O}(e^2)$ whereas $\Theta_3, \Theta_4 \sim \mathcal{O}(1)$. Therefore, given that Θ_1 is constant and small, we will neglect Θ_1 as this has little effect on the dynamics. Expanding the Hamiltonian to second order in $\frac{\Theta_2}{\Theta_3}$ and $\frac{\Theta_2}{\Theta_4}$, and performing a (partial) transformation back to the Poincaré variables using $\Theta_3 \approx \Lambda$ and $\Theta_4 \approx \underline{\Lambda}$, we find that the Hamiltonian describing near resonance behavior is

$$H = \alpha \underline{\Gamma} + \beta \underline{\Gamma}^2 + \kappa \sqrt{2\underline{\Gamma}} \cos \theta_2 + \mathcal{O}\left(\frac{1}{c^4}, f_d^2, e^3\right) \quad (4.15)$$

$$\begin{aligned}
 \alpha &:= j \frac{\mu^3 M^2}{\Lambda^3} + (1-j) \frac{\mu^3 M^2}{\underline{\Lambda}^3} + \frac{1}{c^2} \left[\frac{9}{2} j \frac{\mu^5 M^4}{\Lambda^5} + \frac{3}{2} (1-3j) \frac{\mu^5 M^4}{\underline{\Lambda}^5} \right] \\
 \beta &:= -\frac{3j^2 \mu^3 M^2}{2 \Lambda^4} - \frac{3(1-j)^2 \mu^3 M^2}{2 \underline{\Lambda}^4} + \frac{1}{c^2} \left[-\frac{45}{4} j^2 \frac{\mu^5 M^4}{\Lambda^6} + \frac{3}{4} (1+10j-15j^2) \frac{\mu^5 M^4}{\underline{\Lambda}^6} \right] \\
 \kappa &:= -f_d \frac{\mu \mu^3 M}{\underline{\Lambda}^{5/2}}.
 \end{aligned} \tag{4.16}$$

The constant α measures the proximity to resonance as resonance occurs when the time-derivative of the resonant argument θ_2 vanishes. In the Newtonian limit, it is clear that α measures the proximity to resonance after noting that $\Lambda = \mu \sqrt{Ma}$ and $\Gamma = \mu \sqrt{Ma}(1 - \sqrt{1 - e^2})$ with a the semimajor axis and e the eccentricity of the unperturbed orbit of the object with mass μ around the central massive object M , so that $\alpha_{\text{Newton}} = (1-j)\omega + j\omega$. In fact, due to the gravitational interaction between the two bodies the radial and azimuthal frequencies are not degenerate. Similarly, post-Newtonian corrections also break the degeneracy between the radial and azimuthal frequencies. Therefore, we expect that at post-Newtonian order α can be written as:

$$\alpha = \underline{\omega}_r - j\underline{\omega}_\phi + j\omega_\phi \tag{4.17}$$

To show this is indeed the case, we need to relate the expression for α in terms of the Poincaré variables to the orbital frequencies in the small eccentricity limit (as the Hamiltonian is also derived in the small eccentricity limit). We do this by writing both Λ , $\underline{\Lambda}$ and the orbital frequencies in terms of the gauge-invariant energy of the orbits E , \underline{E} . First, we note that at leading Newtonian order, $\Gamma \sim \mathcal{O}(e^2)$ so that $p_\phi = \Lambda - \Gamma = \Lambda + \mathcal{O}(e^2)$. Therefore, in the small eccentricity limit we can express Λ entirely in terms of E (and similarly $\underline{\Lambda}$)

$$\Lambda = \frac{\mu^{3/2} M}{\sqrt{-2E}} + \frac{1}{c^2} \frac{9}{8} M \sqrt{-2\mu E} + \mathcal{O}\left(\frac{1}{c^4}, e^2\right) \tag{4.18}$$

where we replaced p_ϕ in the post-Newtonian part by its expression in the circular limit, that is, $\Lambda = \mu^{3/2} M / \sqrt{-2E} + \mathcal{O}(c^{-2})$. The orbital frequencies can also be expressed entirely in terms of E . In the small eccentricity limit the relation between ω_r and E in Eq. (4.11) does not change, but ω_ϕ simplifies:

$$\omega_\phi = \frac{(-2E)^{3/2}}{\mu^{3/2} M} \left(1 - \frac{1}{c^2} \frac{9E}{4\mu} \right) + \mathcal{O}\left(\frac{1}{c^4}, e^2\right). \tag{4.19}$$

Writing α in Eq. (4.16) in terms of E and using the expressions for ω_r and ω_ϕ in terms of E , we find that indeed

$$\alpha - (\underline{\omega}_r - j\underline{\omega}_\phi + j\omega_\phi) = \mathcal{O}(c^{-4}, e^2). \tag{4.20}$$

This establishes that the expectation in Eq. (4.17) is correct. It agrees with its fully relativistic counterpart on a Schwarzschild spacetime.

Higher order resonances of order N , that is, of the form $j - N : j$ slightly alter the numerical value of the coefficients α and β and change the power of 2Γ in the interaction Hamiltonian to $(2\Gamma)^{N/2}$. Since $\Gamma \sim \mathcal{O}(e^2)$, this demonstrates why the orbital dynamics are dominated by lower order resonances.

Interior resonances can be treated very similarly. The resulting Hamiltonian will have the same form as in Eq. (4.15), but the constants will be slightly different.

V. RESONANCE CAPTURE, EVOLUTION AND ESCAPE

The capture, evolution and escape of mean motion resonance have been extensively discussed in planetary systems. The capture only happens if it is a converging migration, in which case the ratio between the semimajor axes passes through the resonance value toward one [1]. The migration could be driven by tidal interaction between the planets with the host star, or planets with the protoplanetary disk. The capture is easier if the initial eccentricities of the planets are small, although there are studies showing that large-eccentricity captures are still possible [35]. On the other hand, it has been shown that even when the eccentricities are very small, resonance capture may fail if the migration speed is too fast [36].

After the resonance capture, the locked pair of objects may migrate together within a disk. Depending on the dissipation mechanism, e.g., the disk force, and the system parameters, the resonance is sustained or breaks. The duration of resonances is related to the puzzle that most planets in multiplanet systems observed by *Kepler* spacecraft do not reside in mean motion resonances [28,37]. The analysis in [28] shows that under disk-planet interaction with characteristic semimajor axis damping rate $1/\tau_a$ and eccentricity damping rate $1/\tau_e$, an exterior $j - 1 : j$ resonance is permanently sustained if

$$\eta' > \frac{j-1}{\sqrt{3}j^{3/2}c} \left(\frac{\tau_e}{\tau_a} \right)^{3/2} \tag{5.1}$$

with $c \approx 0.8j$ and η' the mass ratio of the outer object and the central massive object. On the other hand, if

$$\eta' < \frac{(j-1)^2}{8\sqrt{3}j^{3/2}\beta} \left(\frac{\tau_e}{\tau_a}\right)^{3/2} \quad (5.2)$$

the resonance is only sustained for a duration proportional to the eccentricity damping timescale τ_e . If the mass ratio η' resides between the thresholds in Eq. (5.1) and Eq. (5.2), the resonance is permanently sustained with a finite libration amplitude in the phase space.

Applying the insights from planetary dynamics to stellar-mass black holes near massive black holes, we immediately observe that the condition for sustained resonance in Eq. (5.1) is difficult to achieve with purely gravitational radiation damping, in which case τ_e is comparable to τ_a unless the orbit is highly eccentric. Therefore, the astrophysical environment of such systems is critical for sustained resonance to occur. Stellar-mass black holes in galactic nuclei may migrate toward the central massive black hole due to mass segregation effects, dynamical friction and/or interaction with a possible accretion disk around the massive black hole. Here we will consider a scenario with a thin-disk profile around the massive black hole, and two stellar-mass black hole (SBH) orbiting within the disk. Such systems could be found at the center of active galaxies. Studies [38–41] suggest that of all galaxies roughly $\mathcal{O}(1\%)$ – $\mathcal{O}(10\%)$ are active [with active galactic nuclei (AGN)]. Moreover, recently there has been a growing interest in understanding the dynamics of stellar-mass objects within AGN disks as a way to produce heavy stellar-mass black holes through hierarchical mergers [42].

Following the description in [19], we consider two types of thin-disk model: α -disks and β -disks. To the authors' knowledge, it is theoretically not clear which effective description of viscosity better describes reality. A deeper understanding of the underlying mechanism that generates the viscosity is needed. Depending on the assumptions, there are magneto-hydrodynamical simulations which favor the α -disk model [43,44], whereas other simulations are more consistent with the β -disk model [45,46]. Some observation suggested that the spectral constraints are better described by the β -disk model [47]. Therefore we consider both descriptions in this study.

In the α -disk model, the viscous stress is parametrized as $t_{t\phi} = -(3/2)\alpha p_{\text{tot}}$ with $t_{t\phi}$ the viscous shear stress in the azimuthal direction, α a dimensionless constant and p_{tot} the total pressure. The surface density Σ of the α -disk is

$$\Sigma \sim 5.9 \times 10^{-21} M_{\odot}^{-1} \alpha_1^{-1} \dot{m}_{\bullet 1}^{-1} \bar{r}_{10}^{3/2}, \quad (5.3)$$

and the disk scale height H is

$$H \sim 1.5 \times 10^5 M_{\odot} \dot{m}_{\bullet 1} M_{\bullet 5}, \quad (5.4)$$

where we have defined $\alpha_1 := \alpha/(0.1)$, $\bar{r}_{10} := r/(10M)$, $M_{\bullet 5} := M/(10^5 M_{\odot})$, and $\dot{m}_{\bullet 1} := \dot{M}/(0.1\dot{M}_{\text{Edd}})$, with \dot{M}_{Edd} being the Eddington accretion rate. The main difference between α - and β -disks is the description of their viscous stress. For β -disks, the viscous stress is assumed to be $t_{t\phi} = -(3/2)\alpha p_{\text{gas}}$, so that only the gas pressure p_{gas} contributes to the viscous stress instead of the total pressure p_{tot} . As a result, the disk surface density is now given by

$$\Sigma \sim 1.4 \times 10^{-17} M_{\odot}^{-1} \alpha_1^{-4/5} \dot{m}_{\bullet 1}^{3/5} M_{\bullet 5}^{1/5} \bar{r}_{10}^{-3/5}, \quad (5.5)$$

while the disk scale height is the same as Eq. (5.4).

There are two main types of disk-SBH interactions. The first is the accretion-induced force, where the Bondi accretion into the SBH brings in additional momentum and energy. The second force is known as Type I “migration force” and comes from the gravitational interaction between the SBH and the induced density waves in the disk (see discussions on Lindblad and corotational resonance in [48,49]). Both of them predict that (with different C)

$$\begin{aligned} \frac{1}{\tau_a} &= \frac{1}{\omega} \frac{d\omega}{dt} \sim C \eta_d \left(\frac{a}{H}\right)^2 \omega, \\ \frac{1}{\tau_e} &= \frac{1}{e} \frac{de}{dt} \sim C \eta_d \left(\frac{a}{H}\right)^4 \omega, \end{aligned} \quad (5.6)$$

with a being the semimajor axis, $\eta_d = \Sigma a^2/M$ the disk to central black hole mass ratio, and the constants C are $\mathcal{O}(1)$ – $\mathcal{O}(10)$. As the scale height H in thin-disk models is constant, τ_e can be much smaller than τ_a for wide orbits ($a \gg H$), so that Eq. (5.1) is satisfied and mean motion resonance is sustained. For a central black hole with mass $M \sim 10^6 M_{\odot}$ and accretion rate $\dot{m}_{\bullet 1} \sim 1$, the gravitational radiation reaction becomes dominant for $r \leq 100M$ for α -disks and $r \leq 30M$ for β -disks. For radii larger than the critical radius the disk force is more important and sustained locking of the mean motion resonance becomes possible.

In Fig. 5–8 we present the numerical evolution of two SBHs around a supermassive BH, with different initial separation and different disk models. The exact form of the disk force is adapted from Sec. VII.B of [19] for the migration force and Sec. V.A of [19] for the accretion force. The numerical evolution employs the N-body code REBOUND developed in [50,51], where we have added the leading order post-Newtonian corrections to the conservative and dissipative part of equation of motions and the disk force.¹¹ In all these cases, the system is

¹¹There is an important caveat associated with the treatment of β -disks. In principle for the parameters assumed here, the SBHs may open gaps in the disk for $a \geq 100M$. The disk-SBH interaction will be stronger in the presence of a disk cavity. However, it is not clear how to obtain τ_e for an eccentric orbit with a disk cavity. We therefore still use the Type I disk force described in [19] for the numerical evolution.

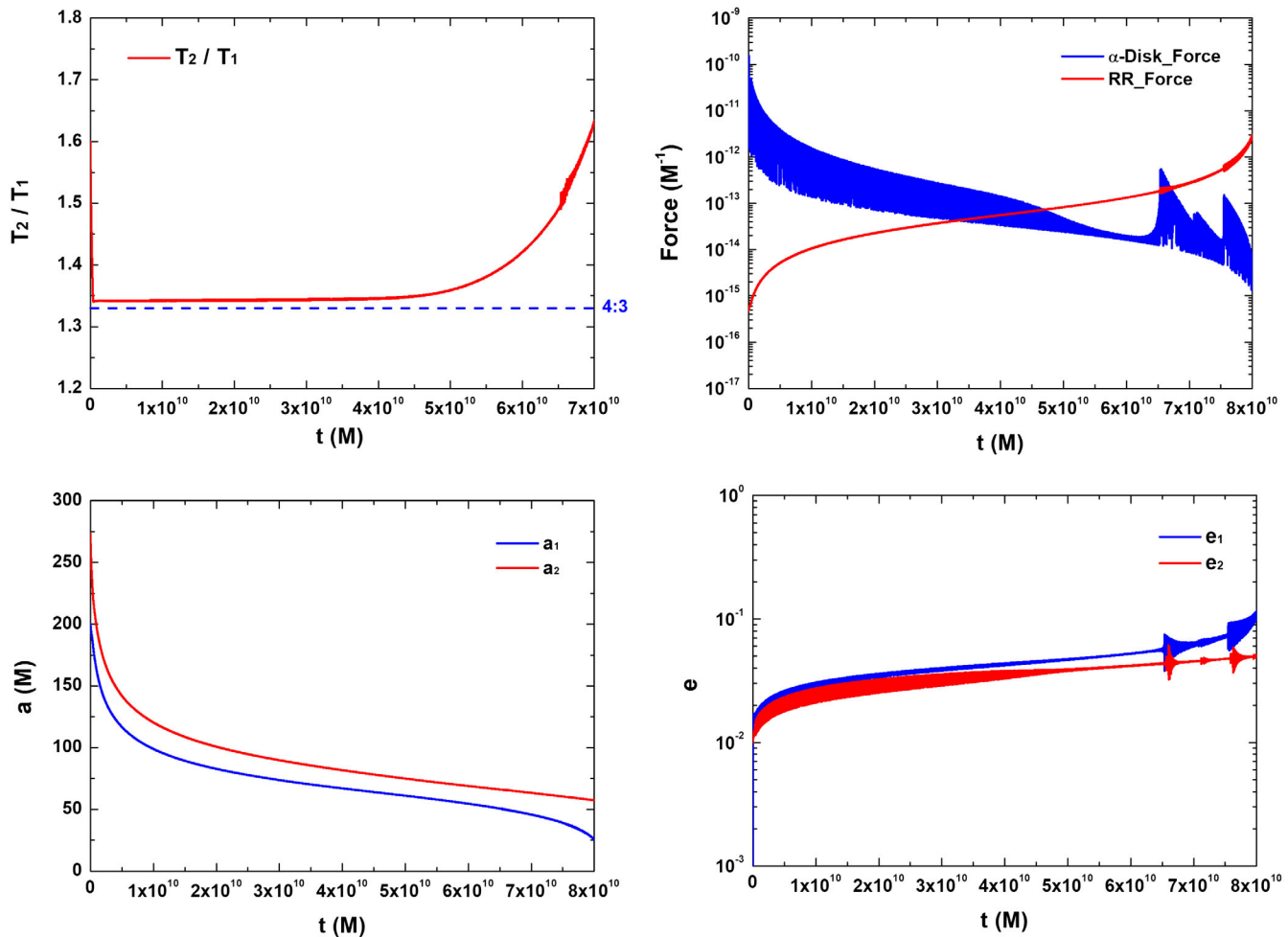


FIG. 5. Orbital evolution with the initial radius a of the inner object equal to $200M$, the semimajor axis \underline{a} of the outer object equal to $273.5828M$ and its eccentricity \underline{e} equal to 0.01. The disk profile is modeled by an α -disk. Top left panel: the ratio between the periods of the two SBHs as a function of time showing that the system is captured into 3:4 resonance. Top right panel: the magnitude of the disk force and the gravitational radiation reaction force experienced by the inner object. The mean motion resonance breaks down roughly at the point that gravitational radiation reaction exceeds the magnitude of the disk force. Bottom left panel: the evolution of semimajor axes with respect to time. Bottom right panel: the evolution of the eccentricities with respect to time.

captured into a $j-1:j$ resonance until the point that the gravitational radiation reaction is greater than the disk force. During the mean motion resonance, the two SBHs migrate together toward the supermassive BH, while keeping the ratio of their periods $(j-1)/j$ roughly constant.

In fact, this system is captured into an inner and outer resonance *simultaneously*. The occurrence of pairs of resonances is not new and has been observed in other scenarios as well [52]. Plots of the resonance angles demonstrating explicitly that the system is indeed captured into both an inner and outer resonance are shown in Appendix B, where we also included a short discussion on a subtle issue regarding the numerical extraction of these resonant angles when the eccentricities are small and post-Newtonian effects are important.

At the point where the mean motion resonance breaks, the outer object has already been brought to a rather close

distance from the supermassive BH. While the inner SBH spirals into the supermassive BH and enters the LISA band, its motion will be affected by the gravitational field of the outer object. In [22,53] it has been shown that the main effect of the external perturber is to modify the angular momentum of the inner inspiraling binary, through an effect referred to as tidal resonance. This effect will be encoded into the gravitational radiation from the inner binary, which may be detected by LISA. It is also important to note that in general the disk rotation does not necessarily align with the spin of the supermassive black hole. In those cases we generally expect inclined extreme mass-ratio inspirals.

The period ratios shown in Fig. 5–8 are a few percent off the exact value $j:j-1$. Similar phenomena has been observed by the *Kepler* spacecraft [37] with many associated discussions in [54–57], although most of the Kepler systems are outside of the mean motion resonances.

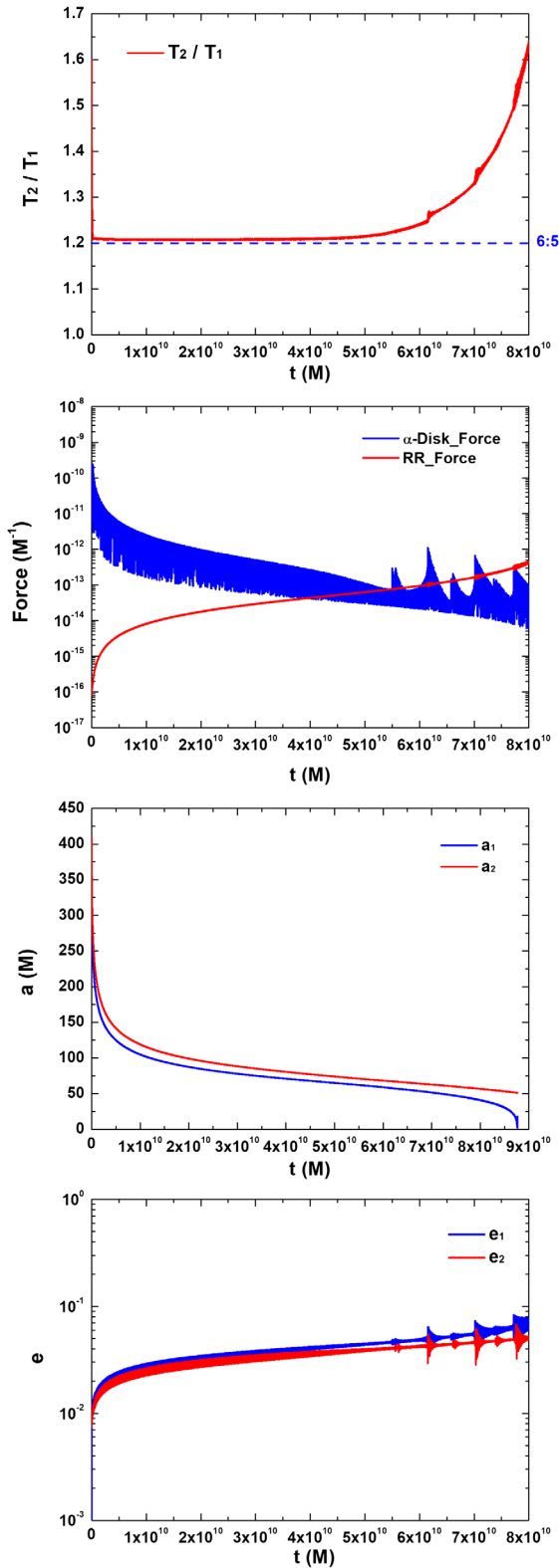


FIG. 6. Similar to Fig. 5, except that the system starts with $a = 300M$ and $\underline{a} = 410.3742M$ and later on is captured into 6:5 resonance. It misses the 3:4 resonance because at that point the migration rate is still too fast [36].

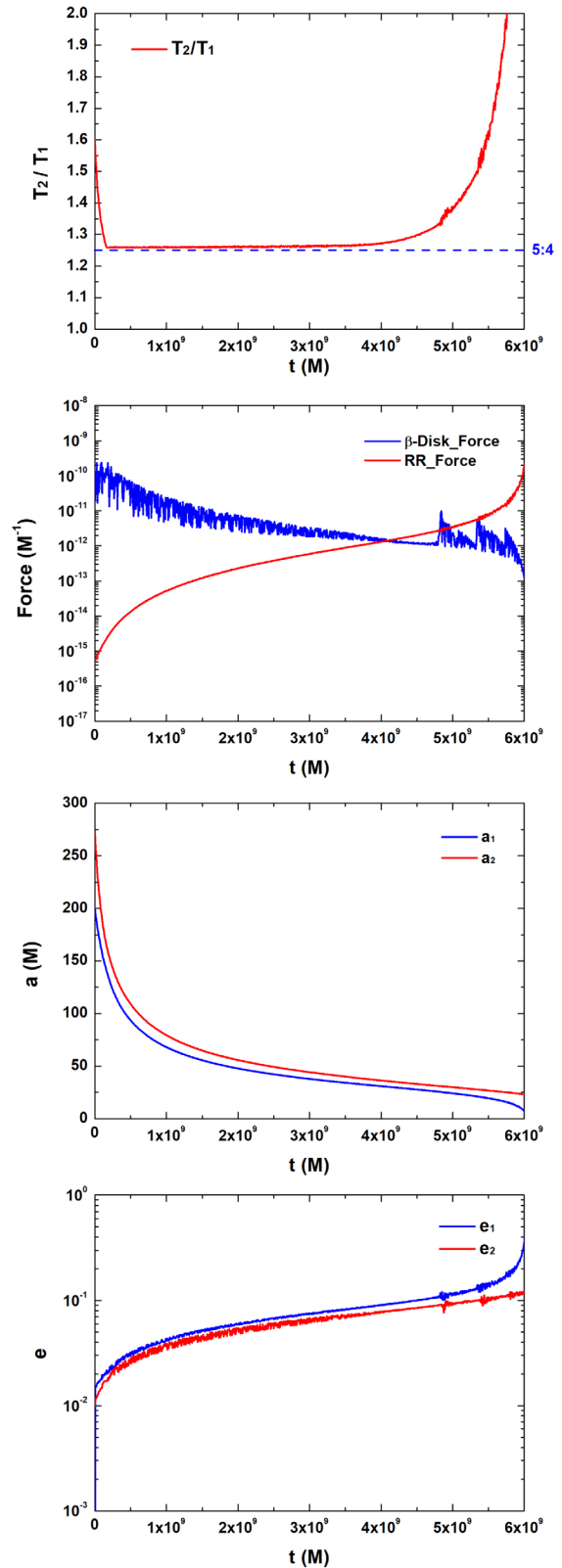


FIG. 7. Similar to Fig. 5, except that the disk profile is a β -disk and later on the system gets captured into 5:4 resonance. It misses the 2:3 and 3:4 resonances because at those points the migration rate is still too fast [36].

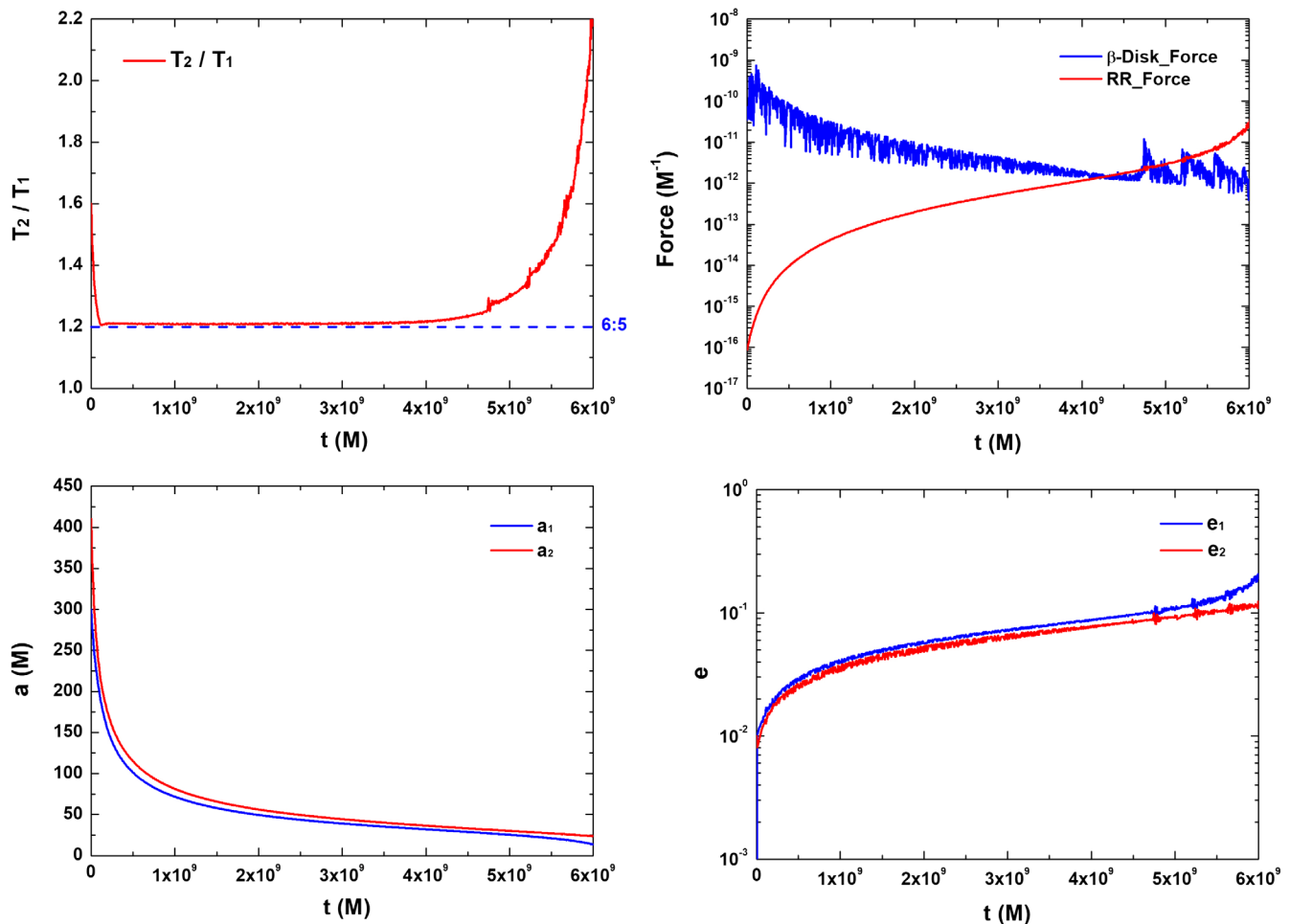


FIG. 8. Similar to Fig. 6, except that the disk profile is a β -disk and later on the system gets captured into 5:6 resonance. It misses the 2:3, 3:4 and 4:5 resonances because at those points the migration rate is still too fast [36].

VI. CONCLUSION

In this work we consider the relativistic generalization of the mean motion resonance widely studied in planetary systems. The primary system of interest is a supermassive black hole with several stellar-mass black holes (SBHs) orbiting in its vicinity. Depending on the distance between the SBHs and the supermassive black hole, relativistic corrections may become important.

We have presented two separate analysis for this multi-body system, depending on the importance of relativistic correction. If the SBHs move within the strong gravity regime of the supermassive BH, the only reliable approach to describe their motion is black hole perturbation theory. In Sec. II we develop a Hamiltonian formalism using black hole perturbation theory, and find much richer structure for mean motion resonance in this fully relativistic regime. In fact, in general each SBH has three orbital frequencies for a Kerr geodesic motion, and the relativistic mean motion resonance could happen if the combination of six orbital frequencies of the two SBHs is zero. Despite the theoretical

interest in such resonance structure, it remains an open question which of these possible mean motion resonances is astrophysically relevant.

In the second approach, as discussed in Sec. IV, we include post-Newtonian corrections to the equation of motion of the multi-body system. This approach is physically more transparent, as one can analytically take the limit $1/c^2 \rightarrow 0$ in the post-Newtonian Hamiltonian and recover the known Newtonian result. However, it only applies for cases in which the post-Newtonian expansion is valid so that it is accurate to truncate the series after the first-order post-Newtonian terms, i.e., away from the strong-gravity regime. We find that the post-Newtonian correction does introduce the precession of the pericenters of the SBHs, but the qualitative structure of the resonances remains unchanged. It is also worth to note that post-Newtonian effects in Kozai-Lidov mechanism have been studied in the past [58–60].

To illustrate possible way(s) to form resonant pairs of SBHs, in Sec. V we have presented a few numerical examples for multi-SBHs moving within a thin accretion

disk around a supermassive black hole. In the regime that the disk force dominates over the gravitational radiation reaction, we observe sustained locking of the mean motion resonance, so that both SBHs migrate to close distances from the supermassive black hole until the gravitational radiation starts to dominate and the resonance breaks down. While this is a viable physical scenario, it remains an open question whether the conditions for this to occur are realized in astrophysical systems. Additionally, there may exist other astrophysical scenarios—not explored here—in which SBH pairs are locked into mean motion resonance within the gravitational influence sphere of a supermassive black hole.

If the resonance breaks down before the inner SBH enters the LISA band, the outer SBH will act as a gravitational perturber to the inner extreme mass-ratio inspiral within the LISA band. Such scenario has been discussed in [22], where the main contribution from the outer SBH is through resonant kicks during tidal resonances [22,53]. On the other hand, if the pair of SBHs is still locked into resonance once the inner SBH enters the LISA band, they must coherently spiral into the supermassive black hole, with the gravitational waveform vastly different from an ordinary extreme mass-ratio waveform. According to the numerical examples studied in Sec. V, such a scenario probably only happens for β -disk models as these models have a much smaller resonance-breaking radius, or for possible SBHs surrounding intermediate mass black holes in dwarf galaxies e.g., [61].

ACKNOWLEDGMENTS

H. Y. and B. B. thank Eric Poisson and Cole Miller for interesting discussions. This research was supported by NSERC and in part by the Perimeter Institute for Theoretical Physics. Research at Perimeter Institute is supported by the Government of Canada through the Department of Innovation, Science and Economic Development Canada and by the Province of Ontario through the Ministry of Research, Innovation and Science.

APPENDIX A: TENSOR HARMONICS

We slightly modify the normalization of the original convention of Zerilli [62] and notation in [32] to evaluate metric perturbations in Sec. III. The relevant tensor components are

$$\mathbf{a}_{\ell m}^{(0)} = \begin{pmatrix} Y_{\ell m} & 0 & 0 & 0 \\ 0 & 0 & 0 & 0 \\ 0 & 0 & 0 & 0 \\ 0 & 0 & 0 & 0 \end{pmatrix}, \quad \mathbf{a}_{\ell m}^{(1)} = \begin{pmatrix} 0 & Y_{\ell m} & 0 & 0 \\ Y_{\ell m} & 0 & 0 & 0 \\ 0 & 0 & 0 & 0 \\ 0 & 0 & 0 & 0 \end{pmatrix}, \quad (\text{A1})$$

$$\mathbf{a}_{\ell m} = \begin{pmatrix} 0 & 0 & 0 & 0 \\ 0 & Y_{\ell m} & 0 & 0 \\ 0 & 0 & 0 & 0 \\ 0 & 0 & 0 & 0 \end{pmatrix}, \quad \mathbf{b}_{\ell m}^{(0)} = \begin{pmatrix} 0 & 0 & \frac{\partial Y_{\ell m}}{\partial \theta} & \frac{\partial Y_{\ell m}}{\partial \phi} \\ 0 & 0 & 0 & 0 \\ \frac{\partial Y_{\ell m}}{\partial \theta} & 0 & 0 & 0 \\ \frac{\partial Y_{\ell m}}{\partial \phi} & 0 & 0 & 0 \end{pmatrix}, \quad (\text{A2})$$

$$\mathbf{c}_{\ell m}^{(0)} = \begin{pmatrix} 0 & 0 & \frac{1}{\sin \theta} \frac{\partial Y_{\ell m}}{\partial \phi} & -\sin \theta \frac{\partial Y_{\ell m}}{\partial \theta} \\ 0 & 0 & 0 & 0 \\ \frac{1}{\sin \theta} \frac{\partial Y_{\ell m}}{\partial \phi} & 0 & 0 & 0 \\ -\sin \theta \frac{\partial Y_{\ell m}}{\partial \theta} & 0 & 0 & 0 \end{pmatrix}, \quad (\text{A3})$$

$$\mathbf{c}_{\ell m} = \begin{pmatrix} 0 & 0 & 0 & 0 \\ 0 & 0 & \frac{1}{\sin \theta} \frac{\partial Y_{\ell m}}{\partial \phi} & -\sin \theta \frac{\partial Y_{\ell m}}{\partial \theta} \\ 0 & \frac{1}{\sin \theta} \frac{\partial Y_{\ell m}}{\partial \phi} & 0 & 0 \\ 0 & -\sin \theta \frac{\partial Y_{\ell m}}{\partial \theta} & 0 & 0 \end{pmatrix}, \quad (\text{A4})$$

$$\mathbf{d}_{\ell m} = \begin{pmatrix} 0 & 0 & 0 & 0 \\ 0 & 0 & 0 & 0 \\ 0 & 0 & -\frac{X_{\ell m}}{\sin \theta} & \sin \theta W_{\ell m} \\ 0 & 0 & \sin \theta W_{\ell m} & \sin \theta X_{\ell m} \end{pmatrix}, \quad (\text{A5})$$

$$\mathbf{g}_{\ell m} = \begin{pmatrix} 0 & 0 & 0 & 0 \\ 0 & 0 & 0 & 0 \\ 0 & 0 & Y_{\ell m} & 0 \\ 0 & 0 & 0 & \sin^2 \theta Y_{\ell m} \end{pmatrix}, \quad (\text{A6})$$

$$\mathbf{f}_{\ell m} = \begin{pmatrix} 0 & 0 & 0 & 0 \\ 0 & 0 & 0 & 0 \\ 0 & 0 & W_{\ell m} & X_{\ell m} \\ 0 & 0 & X_{\ell m} & -\sin^2 \theta W_{\ell m} \end{pmatrix}. \quad (\text{A7})$$

The tensor harmonic functions are

$$X_{\ell m} = 2 \frac{\partial}{\partial \phi} \left(\frac{\partial}{\partial \theta} - \cot \theta \right) Y_{\ell m},$$

$$W_{\ell m} = \left(\frac{\partial^2}{\partial \theta^2} - \cot \theta \frac{\partial}{\partial \theta} - \frac{1}{\sin^2 \theta} \frac{\partial^2}{\partial \phi^2} \right) Y_{\ell m}. \quad (\text{A8})$$

APPENDIX B: RESONANT ANGLES

In order to verify that a given system indeed resides in one (or more) mean motion resonances, it is important to check whether the corresponding resonant angles $\theta_{1,2}$ librate around a constant value. Surprisingly, even when the period ratios are clearly locked near $j-1:j$ in Fig. 5–8, there is no sign of resonant angle locking given an instantaneous extraction of the resonant angles. Interestingly, if we

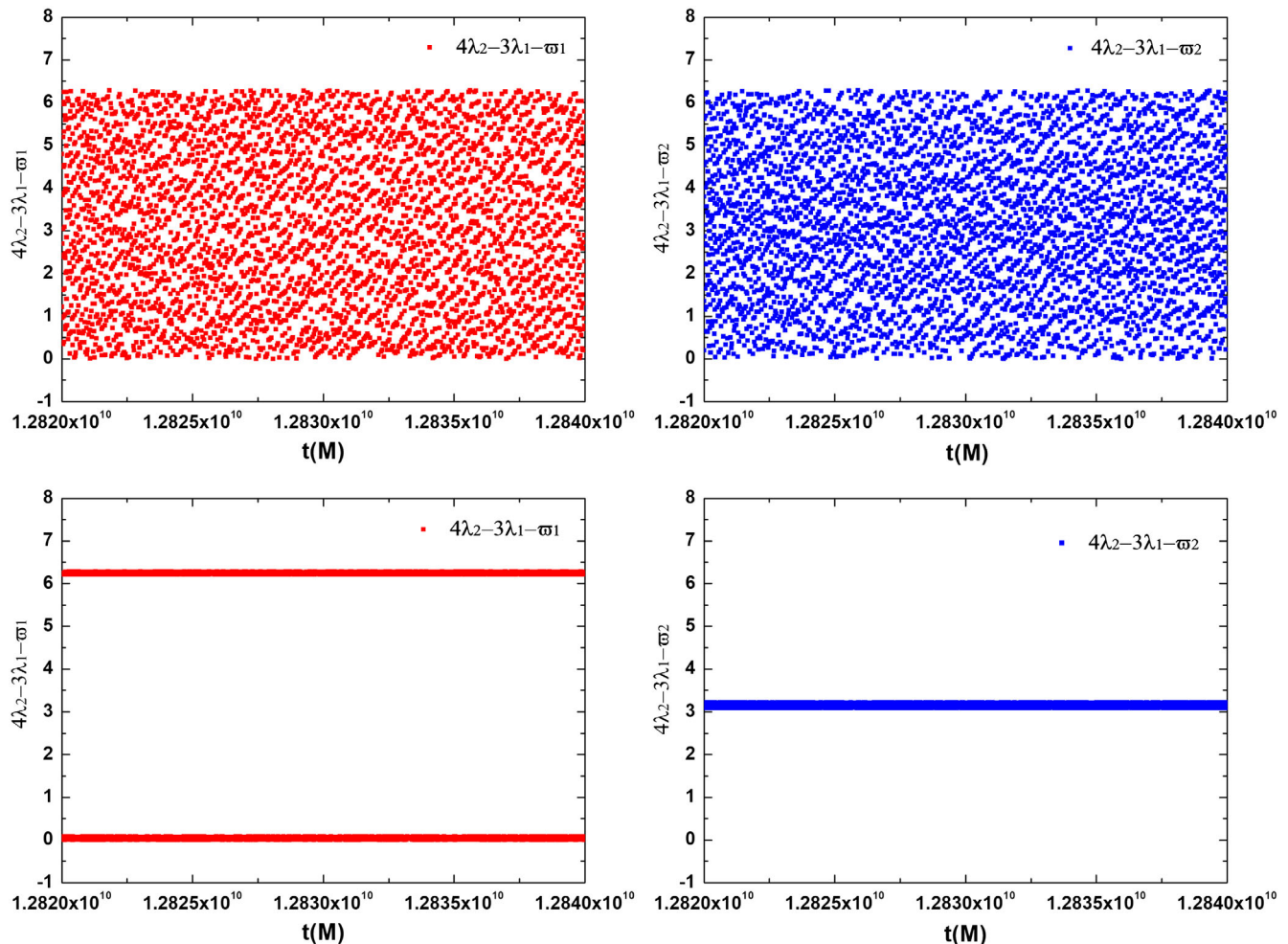


FIG. 9. Top left/right panel: Resonant angles θ_1/θ_2 of the osculating orbit corresponding to the simulation shown in Fig. 5 during a representative time frame after the ratio of the period is roughly 4 : 3. We do not observe locking of the resonant angles. Bottom left/right panel: Removing the IPN term that generates the general relativistic precession, resonant angle locking is restored. (In order to be consistent to the literature in planetary science [1], we denote the argument of pericenter as ϖ , which is just $-\gamma$ in Sec. IV.)

remove the first post-Newtonian Hamiltonian in the equation of motion and perform the simulation again, the resonant angle locking is clearly restored, as shown in Fig. 9. Naively, this seems to suggest that post-Newtonian corrections prohibit the system from entering into mean motion resonance. This is not correct: the system does experience mean motion resonance. The resolution is provided by how the resonant angles are extracted from the data.

It turns out that it has been long known that post-Newtonian corrections to the equations of motion may give rise to “perpetual precession” when the eccentricity is small [63,64].¹² In other words, for small eccentricities the precession rate induced by the post-Newtonian corrections becomes the same as the orbital frequency, and as a result

¹²This effect is not unique to post-Newtonian theory and other “strange” behaviors when eccentricities are small have also been studied in the planetary science community, see [64] for references.

the true anomaly stays roughly constant in the post-Newtonian osculating description. In such cases, the physical orbits can be circular even if the osculating orbit is eccentric. This is exactly what is happening here. From the data we extract from REBOUND where the Poincaré variables are obtained by fitting instantaneous motion by elliptical orbits (the “osculating orbit” approximation), we do observe that the true anomaly stays approximately constant ($\sim\pi$) and the precession rate is the same as the orbital frequency. On the other hand, the physical eccentricity—measured by comparing the maximum and minimum distance from the supermassive black hole on orbital timescales—is on the order of 10^{-3} in contrast to the osculating eccentricity that is on the order of 10^{-2} .

In Fig. 10 we drop the osculating orbit assumption and extract the angles from the physical orbit. The corresponding resonant angles of the physical orbits are clearly locked, also when post-Newtonian corrections are included. This also explains why the period ratio stays constant during resonance.

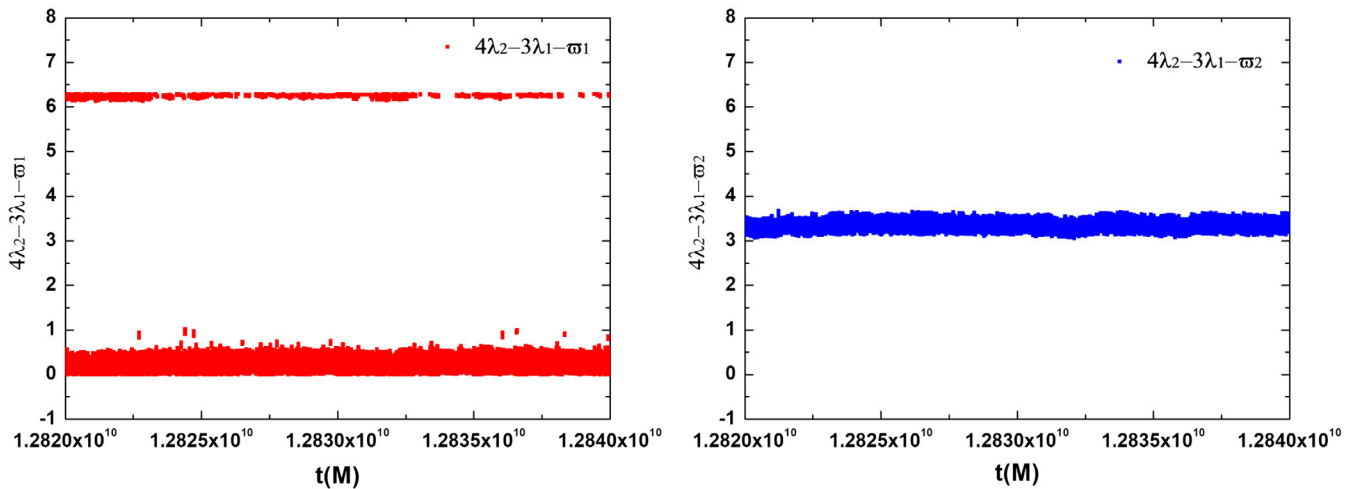


FIG. 10. Resonant angles θ_1 and θ_2 of the physical orbit corresponding to the simulation shown in Fig. 5. The resonant angles are both locked in this case.

-
- [1] C. Murry and S. Dermott, *Solar System Dynamics*, 1st ed. (Cambridge University Press, Cambridge, England, 1999).
- [2] J. Williams and G. Benson, *Astron. J.* **76**, 167 (1971).
- [3] Q. Yu and S. Tremaine, *Astron. J.* **118**, 1873 (1999).
- [4] J. Wisdom, *Astron. J.* **87**, 577 (1982).
- [5] S. F. Dermott and C. D. Murray, *Nature (London)* **301**, 201 (1983).
- [6] S. M. Mills, D. C. Fabrycky, C. Migaszewski, E. B. Ford, E. Petigura, and H. Isaacson, *Nature (London)* **533**, 509 (2016).
- [7] S. A. Hughes, in *AIP Conf. Proc.* **873**, 233 (2006).
- [8] S. Alexander and N. Yunes, *Phys. Rep.* **480**, 1 (2009).
- [9] D. J. Gross and J. H. Sloan, *Nucl. Phys.* **B291**, 41 (1987).
- [10] H. Miao, H. Yang, and D. Martynov, *Phys. Rev. D* **98**, 044044 (2018).
- [11] D. Martynov, H. Miao, H. Yang, F. H. Vivanco, E. Thrane, R. Smith, P. Lasky, W. E. East, R. Adhikari, A. Bauswein *et al.*, *Phys. Rev. D* **99**, 102004 (2019).
- [12] J. Zhang and H. Yang, *Phys. Rev. D* **99**, 064018 (2019).
- [13] J. Zhang and H. Yang, [arXiv:1907.13582](https://arxiv.org/abs/1907.13582) [*Phys. Rev. D* (to be published)].
- [14] O. A. Hannuksela, K. W. Wong, R. Brito, E. Berti, and T. G. Li, *Nat. Astron.* **3**, 447 (2019).
- [15] R. Brito, S. Ghosh, E. Barausse, E. Berti, V. Cardoso, I. Dvorkin, A. Klein, and P. Pani, *Phys. Rev. D* **96**, 064050 (2017).
- [16] V. Cardoso, E. Franzin, and P. Pani, *Phys. Rev. Lett.* **116**, 171101 (2016).
- [17] V. Cardoso, E. Franzin, A. Maselli, P. Pani, and G. Raposo, *Phys. Rev. D* **95**, 084014 (2017).
- [18] A. Maselli, P. Pani, V. Cardoso, T. Abdelsalhin, L. Gualtieri, and V. Ferrari, *Phys. Rev. Lett.* **120**, 081101 (2018).
- [19] B. Kocsis, N. Yunes, and A. Loeb, *Phys. Rev. D* **84**, 024032 (2011).
- [20] E. Barausse, V. Cardoso, and P. Pani, *Phys. Rev. D* **89**, 104059 (2014).
- [21] N. Yunes, M. Coleman Miller, and J. Thornburg, *Phys. Rev. D* **83**, 044030 (2011).
- [22] B. Bonga, H. Yang, and S. A. Hughes, *Phys. Rev. Lett.* **123**, 101103 (2019).
- [23] E. Poisson, A. Pound, and I. Vega, *Living Rev. Relativity* **14**, 7 (2011).
- [24] L. Barack and A. Pound, *Rep. Prog. Phys.* **82**, 016904 (2019).
- [25] H. Yang, F. Zhang, A. Zimmerman, and Y. Chen, *Phys. Rev. D* **89**, 064014 (2014).
- [26] H. Yang, D. A. Nichols, F. Zhang, A. Zimmerman, Z. Zhang, and Y. Chen, *Phys. Rev. D* **86**, 104006 (2012).
- [27] L. Barack, *Classical Quantum Gravity* **26**, 213001 (2009).
- [28] P. Goldreich and H. E. Schlichting, *Astron. J.* **147**, 32 (2014).
- [29] M. van de Meent, *Phys. Rev. D* **89**, 084033 (2014).
- [30] J. Kevorkian and J. D. Cole, *Multiple Scale and Singular Perturbation Methods (Applied Mathematical Sciences)* (Springer Verlag, New York, 1996).
- [31] S. Jhingan and T. Tanaka, *Phys. Rev. D* **67**, 104018 (2003).
- [32] N. Sago, H. Nakano, and M. Sasaki, *Phys. Rev. D* **67**, 104017 (2003).
- [33] L. Blanchet, *Living Rev. Relativity* **9**, 4 (2006).
- [34] S. J. Peale, *Annu. Rev. Astron. Astrophys.* **14**, 215 (1976).
- [35] X. Wang and R. Malhotra, *Astrophys. J.* **848**, 20 (2017).
- [36] L. Friedland, *Astrophys. J. Lett.* **547**, L75 (2001).
- [37] D. C. Fabrycky, J. J. Lissauer, D. Ragozzine, J. F. Rowe, J. H. Steffen, E. Agol, T. Barclay, N. Batalha, W. Borucki, D. R. Ciardi *et al.*, *Astrophys. J.* **790**, 146 (2014).
- [38] B. Lehmer, D. Alexander, J. Geach, I. Smail, A. Basu-Zych, F. Bauer, S. Chapman, Y. Matsuda, C. Scharf, M. Volonteri *et al.*, *Astrophys. J.* **691**, 687 (2009).

- [39] B. Lehmer, A. Lucy, D. Alexander, P. Best, J. Geach, C. Harrison, A. Hornschemeier, Y. Matsuda, J. Mullaney, I. Smail *et al.*, *Astrophys. J.* **765**, 87 (2013).
- [40] J. Digby-North, K. Nandra, E. Laird, C. Steidel, A. Georgakakis, M. Bogosavljević, D. Erb, A. Shapley, N. Reddy, and J. Aird, *Mon. Not. R. Astron. Soc.* **407**, 846 (2010).
- [41] M. Macuga, P. Martini, E. D. Miller, M. Brodwin, M. Hayashi, T. Kodama, Y. Koyama, R. A. Overzier, R. Shimakawa, K.-i. Tadaki *et al.*, *Astrophys. J.* **874**, 54 (2019).
- [42] Y. Yang, I. Bartos, V. Gayathri, K. Ford, Z. Haiman, S. Klimentko, B. Kocsis, S. Márka, Z. Márka, B. McKernan *et al.*, *Phys. Rev. Lett.* **123**, 181101 (2019).
- [43] K. Ohsuga, S. Mineshige, M. Mori, and Y. Kato, *Publ. Astron. Soc. Jpn.* **61**, L7 (2009).
- [44] S. Hirose, J. H. Krolik, and O. Blaes, *Astrophys. J.* **691**, 16 (2009).
- [45] N. Turner, J. Stone, and T. Sano, *Astrophys. J.* **566**, 148 (2002).
- [46] N. Turner, *Astrophys. J. Lett.* **605**, L45 (2004).
- [47] C. Done and S. W. Davis, *Astrophys. J.* **683**, 389 (2008).
- [48] P. Goldreich and S. Tremaine, *Astrophys. J.* **233**, 857 (1979).
- [49] P. Goldreich and S. Tremaine, *Astrophys. J.* **241**, 425 (1980).
- [50] H. Rein and S.-F. Liu, *Astron. Astrophys.* **537**, A128 (2012).
- [51] H. Rein and D. S. Spiegel, *Mon. Not. R. Astron. Soc.* **446**, 1424 (2015).
- [52] Y. Matsumoto, M. Nagasawa, and S. Ida, *Icarus* **221**, 624 (2012).
- [53] H. Yang and M. Casals, *Phys. Rev. D* **96**, 083015 (2017).
- [54] Y. Lithwick and Y. Wu, *Astrophys. J. Lett.* **756**, L11 (2012).
- [55] K. Batygin and A. Morbidelli, *Astron. J.* **145**, 1 (2013).
- [56] C. Petrovich, R. Malhotra, and S. Tremaine, *Astrophys. J.* **770**, 24 (2013).
- [57] C. Baruteau and J. C. Papaloizou, *Astrophys. J.* **778**, 7 (2013).
- [58] M. C. Miller and D. P. Hamilton, *Astrophys. J.* **576**, 894 (2002).
- [59] C. M. Will, *Phys. Rev. D* **96**, 023017 (2017).
- [60] S. Naoz, B. Kocsis, A. Loeb, and N. Yunes, *Astrophys. J.* **773**, 187 (2013).
- [61] J.-H. Woo, H. Cho, E. Gallo, E. Hodges-Kluck, H. A. N. Le, J. Shin, D. Son, and J. C. Horst, *Nat. Astron.* **3**, 755 (2019).
- [62] F. J. Zerilli, *Phys. Rev. D* **2**, 2141 (1970).
- [63] C. W. Lincoln and C. M. Will, *Phys. Rev. D* **42**, 1123 (1990).
- [64] C. M. Will, *Classical Quantum Gravity* **36**, 195013 (2019).